12-2021

The Impacts and In-Depth Study of the Environmental Contaminant, Perfluorooctane Sulfonic Acid, and Its Interactions with Water

Karla Veronica Salazar
The University of Texas Rio Grande Valley

THE IMPACTS AND IN-DEPTH STUDY OF THE ENVIRONMENTAL CONTAMINANT, PERFLUOROOCTANE SULFONIC ACID, AND ITS INTERACTIONS WITH WATER

A Thesis

by

KARLA VERONICA SALAZAR

Submitted in Partial Fulfillment of the

Requirements for the Degree of

MASTER OF SCIENCE

Major Subject: Chemistry

The University of Texas Rio Grande Valley

December 2021

THE IMPACTS AND IN-DEPTH STUDY OF THE ENVIRONMENTAL CONTAMINANT, PERFLUOROOCTANE SULFONIC ACID, AND ITS INTERACTIONS WITH WATER

A Thesis
by
KARLA VERONICA SALAZAR

COMMITTEE MEMBERS

Dr. Wei Lin
Committee Chair

Dr. Shervin Fatehi
Committee Member

Dr. Evangelia Kotsikorou
Committee Member

Dr. Shizue Mito
Committee Member

Dr. Arnulfo Mar
Committee Member

December 2021

ABSTRACT

Salazar, Karla Veronica, The Impacts and In-depth Study of the Environmental Contaminant, Perfluorooctanesulfonic Acid, and its Interactions with Water. Master of Science (MS), December, 2021, 90 pp., 15 tables, 39 figures, references, 116 titles.

Perfluorooctanesulfonic acid (PFOS), similar to perfluorooctanoic acid (PFOA), is a synthetic chemical that has been classified as a persistent organic pollutant (POP) by the Stockholm Convention since 2009. Due to the wide previous usage, high stability, high bio-accumulative, and low degradative properties is the reason that PFOS has been found in several compartments of the environment including ocean water, ground water, air, and sediments. Due to the strong interactions generated by the sulfonic acid end, this compound has a tendency to stay in the environment for long periods of time and has proved to be difficult in the removal from water. This is alarming due to the persistent bioaccumulation of PFOS in the environment leading to further bioaccumulation into animals and humans. This thesis is composed of two projects revolving around PFOS. The first project involves an environmental contaminant survey done in Putian, China. A total of 57 locations were tested that consisted of both, seawater and ground water. In this project, several environmental contaminants, with the inclusion of PFOS, were tested in order to create a baseline documentation for the Putian region in southern China. The main instrumentation used for the detection of PFOS and PFOA was the Solid Phase Extraction (SPE) Enrichment with Ultra High-Performance Liquid Chromatography-Tandem Mass Spectrometry.

The second project focuses on the further study of PFOS by studying a smaller and similarprototype molecule, fluorosulfonic acid. Flourosulfonic acid and its complex hydrates are quantum chemically studied theoretically and experimentally to understand the natural behavior of the first solvation shell of fluorosulfonic acid in the environment. The experimental portion of this researchis done by using a Chirped-Pulse Fourier Transform microwave spectrometer for the monomer and a cavity-based Fourier Transform microwave spectrometer for the complex hydrates. The computational results are carried out through the cluster computers at the Texas Advanced Computer Center (TACC) located in Austin, Texas. The methods used for the theoretical portion include Density Functional Theory (DFT), second order Møller-Plesset Perturbation Theory (MP2), and the Coupled-Cluster Single Double Triple CCSD(T) Theory with the aug-cc-pVTZ basis set. The completion of this research project will give strong, detailed, and accurate information on the core of the problem for perfluorooctanesulfonic acid (PFOS) to help the future removal of this environmental contaminant.

DEDICATION

This thesis wouldn't have been possible without the help and support from my family. Specially, I would like to dedicate this thesis and all my hard work to my mother, Veronica Gomez Leal, my father, Jose Alberto Salazar Sanchez, and my brother, Luis Alberto Salazar. I am so grateful for everything they had to sacrifice in order for me to be able to excel in my education. In addition, I'd also like to thank and dedicate this thesis to the people that helped make this thesis possible. These individuals are Dr. Wei Lin for mentoring me all the way through my thesis, Michael J. Carrillo for all the guidance and knowledge, my pharmacy manager, Cristina Gracia for her support about school while working, and my coworkers for the fillings they had to do whenever I needed to be present in school. Moreover, I'd like to thank and dedicate my work to Dr. Parwinder Grewal, the Executive Vice President for Research, Graduate Studies, and New Program Development for granting me with the sustainability fellowship, Mrs. Marianella Franklin, Chief of sustainability for teaching me about sustainability, showing me her passion for a sustainable future, and for driving me to my limits to deliver an amazing quality of work to make the world a more sustainable place in a future, Forrest Sparks, the sustainability program specialist for his guidance and feedback, and Sandra Montalvo, the sustainability program specialist for her support. I'd also like to thank all the professors that agreed to being in my committee. Last, but not least, I'd like to thank my boyfriend (and future husband), Diego Rodriguez for all the support, the love, and the motivation that helped me get through my master's degree.

ACKNOWLEDGMENTS

I would like to acknowledge the following people for the help they have provided me to make this thesis possible. First and foremost, I'd like to acknowledge my mother, father, brother for the love and support. Following them, I'd like to thank my grandparents from both sides of my mom and dad, my cousins, aunts, uncles, and distant cousins. I also owe major gratitude and would like to acknowledge my friends that helped me be a better person and pushed me to dedicate majorly to school while getting through middle school, and high school. This would include Alma N. Robledo and Nahari Y. Leija. I would like to also thank all of my teachers that taught me and exposed me to so much knowledge. Amongst the earlier teachers, I remember Mrs. McCleary from Chemistry AP in high school. I am very grateful she sparked my interest in chemistry because my educational career with chemistry started with her. Thanks to the material she taught me in high school, I was well prepared for my entrance in college as a chemistry major. Following her, I'd like to thank all the professors that taught me in college in all different areas of chemistry. This includes Ms. Zohra Azim (Gen Chem), Dr. Henry Moore (Ochem), Dr. Shizue Mito (Ochem, Advanced Ochem), Dr. Chen Lin (Ochem), Dr. Bhupendra Srivastava (Ochem), Dr. Arnulfo Mar (Chem Problems), Dr. Hassan Ahmad (Biochem), Dr. Jason Parsons (Analytical, Instrumental, Inorganic, Advanced Chem, Grad Aquatic chem), Dr. Elamin Ibrahim (Instrumental), Dr. Abdurrahman Atesin (Inorganic), Dr. Evangelia Kotsikorou (Pchem, Grad pchem), Dr. Shervin Fatehi (Pchem, Grad pchem elective), and Dr. Javier Macossay (Grad Ochem Elective). I'd also

like to thank my committee for being so supportive. This includes Dr. Arnulfo Mar, Dr. Evangelia Kotsikorou, Dr. Shervin Fatehi, and Dr. Shizue Mito. Last but not least, I'd like to give the most special thanks and acknowledgement to my graduate research advisor, Dr. Wei Lin. I am really grateful for all the knowledge, guidance, and care that came from you to adopt me into your research lab as a graduate student. I learned so much with you. It is unfortunate that the pandemic came and disrupted our lab research plan initially. However, we still were able to move forward due to your excellent guidance to your research group. I am looking forward to being kept in touch with you as I advance in my chemical career. Thank you for everything you have done to help me succeed in getting through a master's degree. I will be forever grateful to you. I'd also like to thank the students that are part of Dr. Lin's research group that were always really nice and supportive. These individuals include Michael Carrillo, Jon, Patrice, Alitza Gracia, Zayra Gonzalez, and Joely Gonzalez, Alonzo Sanchez, and Keila Murillo. I'd like to thank acknowledge my fiancé, Diego Rodriguez, for his support. To conclude, I'd like to thank and acknowledge Dr. Parwinder Grewal, Mrs. Marianella Franklin, Forrest Sparks, and Sandra Montalvo for their help and support.

TABLE OF CONTENTS

LIST OF TABLES

LIST OF FIGURES

CHAPTER I

INTRODUCTION TO PERFLUOROSULFONIC ACID AND IMPACTS

1.1 Introduction

The focus of this research is on the toxic and synthetic organic environmental contaminant, Perfluorooctanesulfonic acid, also known as PFOS. The production of PFOS in the manufacturing industry potentially started as early as the 1950's [112]. Due to its convenient characteristics such as heat, water, oil and degradation resistance, PFOS has been used to make several different products [47]. Some of these products include fire-fighting foam, floor polishes, pesticides and shampoo as seen in Figure 1 [14, 29, 57, 111].

Figure 1: Manufactured Products from PFOS

Since the 1950's, the previous wide usage of PFOS in the manufacturing industry led to the inevitable release of high amounts of this contaminant into the environment [47]. Consequently, PFOS is now found to be bioaccumulated in diverse regions all around the world in several compartments of the environment such as in several bodies of waters, air, plants, and soils [101]. Due to the high molecular stability and low degradative properties, this toxic molecule

has lasted a long time in the environment and has eased a further bioaccumulation in the blood and biological systems of animals and humans [56, 79, 107]. Recently in 2017, it was stated that an average of 20 to 30 μg/L of PFOS has been found in human blood worldwide [1]. In addition, it was reported that the average half-life of PFOS in the blood is of approximately 5 years, emphasizing the long persistency of PFOS in the human system [110]. Having this toxic molecule around in the environment can have several potential sustainable impacts. The impacts that will be discussed in this thesis for PFOS include the social, environmental, and economic impacts.

1.2 Social Impact

Social impacts of PFOS involve several potential health complications including hepatoxicity, endocrine disruptions, neurotoxicity, reproductive toxicity, neonatal death, developmental disorders in fetuses, immunotoxicity, thyroid disruption, cardiovascular toxicity, pulmonary toxicity, renal toxicity, carcinogenesis, and death as shown in Figure 2. [41, 55, 60] In a previous research, it was reported that PFOS mainly targets the liver and causes hepatoxicity due to the inhibition of the β-oxidation of fatty acid that lead to an ease of accumulation of fat in the liver. This accumulation of fat can worsen conditions for those individuals that are already dealing with liver diseases such as high cholesterol and can potentially increase the risk of getting more liver diseases such as hepatic steatosis [113]. Another study also reported that PFOS can alter the immune system by reducing the quantity of lymphocytic, lymphocytes and blood cells. The disruption of the components of the immune system can lead to an ease of acquirement to new diseases and even death due to the lack of immune defense. An example would be with the novel COVID-19 virus spreading and harming hundreds of thousands of people. People who get most affected by the COVID-19 virus are those who are immune-suppressed or have previous pre-existing conditions [48]. Other health complications potentially

caused by PFOS include the impairment of the structure and disruption of the thyroid function, the cytotoxicity and disorder the thyroid hormones, potential cardiac malformation, irregularities of the heart rate, the induction of apoptosis of the cardiomyocyte, alteration of the gene expressions that secrete and transport the proteins and lipids in the lungs, renal toxicity, and disruption of the protection of renal cells [115]. Just like all these health alterations, PFOS can also alter and damage the endocrine, neurological, and the reproductive system.

Figure 2: Health toxicities potentially generated by PFOS

PFOS can bioaccumulate and induce alterations to people of all different ages through different dietary intakes as shown in Figure 3 [21]. It has been reported that mainly PFOS bioaccumulation comes from seafood, followed by fruits and meat. Regardless, PFOS bioaccumulation also comes from eggs, vegetables, milk, sugar, and drinking water. Even infants, from a very early age, can start bioaccumulating PFOS in their blood from drinking water. Other research report also stated that since early stages of pregnancy, PFOS can flow from the mother to the fetus through the umbilical cord [77]. This can cause harm to the baby by potentially causing neonatal developmental disorders or death.

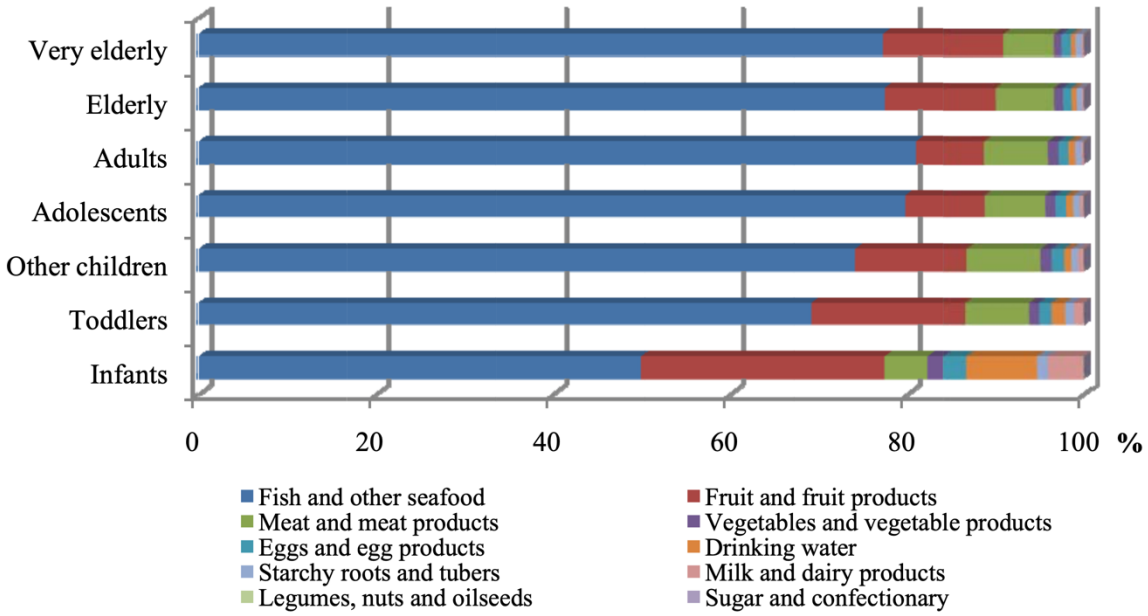

Figure 3: Sources of PFOS bioaccumulation in dietary intakes

As mentioned previously, the average concentration of PFOS found globally is of 20 to 30 μg/L. In Figure 4, a global map of PFOS blood bioaccumulation can be observed [1]. The lighter countries show the countries least affected and the darker countries symbolize the countries most affected by PFOS blood bioaccumulation in the blood. As it can be seen, the United States is one of the most affected countries worldwide along with China, Japan, Australia, Canada and a few others more. This project is taking the first step into making sure this toxic molecule gets completely removed from the environment in a future and prevent further bioaccumulation in the blood for the benefit of future generations.

Figure 4: Global map of PFOS average bioaccumulation in the blood.

1.3 Environmental Impacts

Environmental impacts of PFOS include the massive bioaccumulation since the 1950's into the environment and a variety of animals. According to a global study of perfluorinated compounds in the oceans, it was reported that PFOS was detected in about 80% of the samples taken in the north and mid-Atlantic Ocean, central to eastern Pacific Ocean, and other bodies of water near Japan, China, and Korea. The concentrations that were determined ranged from 338 to 57,700 pg/L in PFOS [107]. Another study, surveyed perfluorinated compounds in the artic environment. Results showed that PFOS was determined to be in a range from 0.02 to 0.97 pg/m^3 in air samples, 1.4 to 4.6 pg/L in snow, 1.2 to 1.8 ng/L in lakes, 24 to 85 ng/g in lake sediments, 10 to 90 pg/L in Greenland seawater, a mean of 20 pg/L in the Labrador Sea, 10 to 424 pg/L from the McClintock channel to Kuujjuarapik, and a mean of 1.22 ng/L in sewage. In addition, it was noted that a variety of animals tested for perfluoro compounds had PFOS bioaccumulation in their system [8].

Detected levels of PFOS in marine animals include 1.8 ng/g for Zooplanktons, 0.28 ng/g in clams, 3.85 ng/g in ice amphipods, a range from 2.0 to 2.5 ng/g of Faroese fish, 0.85 ng/g in atlantic cod, 10.9 ng/g in whales, 2.4 ng/g in Canadian artic walrus, 2.8 ng/g in Otter, 16 ng/g in Holman Ringed seals, a range from 27.9 to 95.6 ng/g in Greenland Ringed seals, and a range from 6.5 ng/g to 88.8 ng/g in Canadian arctic seals. In freshwater, fish concentrations ranged from 5.7 ng/g to 39.9 ng/g from the white sucker to the brook trout. In other animals, PFOS was determined in a concentration of 34 ng/g and 350 ng/g in Alaskan polar bears' blood and liver, an average of 20 ng/g in birds such as the common loon, 250 ng/g of the arctic fox, and a range from 3.8 to 24.4 ng/g of Caribou [8]. Regardless, whether they are water, snow, air, or ground type of animals, they all got greatly affected by this toxic contaminant.

Another research article published in 2009 reports on a tragedy event happening with the bottlenose dolphins around the late 1980's. During these years, about 50% of all the near-shore bottlenose dolphins were found dead. This event then repeated itself two years later along the United States Gulf of Mexico Coast. Studies in the dolphins showed that they suffered a quick spread of infection due to the immune system suppression caused by a significant number of contaminants altering their system. From deeper studies, it was discovered that the PFOS was found in much higher concentrations in the affected dolphins in comparison to those dolphins that were not affected [41].

Figure 5 shows all components that PFOS disrupts, alters, and bioaccumulates in. The center shows the main components of the world. These include the air, the water, the land systems and the life. From those 4 centered pictures, it expands to pictures of animals and humans that also get affected by PFOS. In order to prevent further bioaccumulation into the expansion of the next generations of earth, animals, and humans, environmental contaminants must be removed. If

further accumulation of this toxic chemical continues in the environment, it could get to lethal levels for all living organisms.

Figure 5: Environmental components affected by PFOS.

1.4 Economic Impact

Currently, there has not been much information of economic impacts because this toxic contaminant is not well-known. However, there is some economical information related to PFOS that include testing costs, corporate losses and annual disease costs for several diseases in the United States. There are three different types of testing costs available when discussing Perfluoroalkyl acid contaminants, including PFOS, shown in Figure 6. If people want to test themselves the water that is being used at home, then a testing kit is available for $75 [74]. In case people wanted to have their drinking water tested in a professional laboratory, then the cost can increase up to $600 [43]. Moreover, if people wanted to test how much of PFOS is contained in their blood system, then the cost could increase up to $800 [92]. Since PFOS, as well as other organic contaminants are not well-known, then it is highly expected that the testing would be

arranged separately with an external laboratory in part from the primary care physician and it would also be highly expected for the insurance not to cover the blood test.

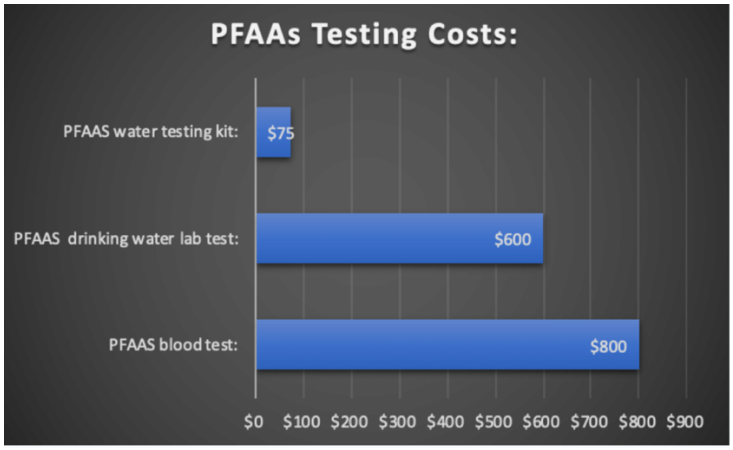

Figure 6: Testing costs of Perfluoroalkyl acids

Another economical shocking impact related to the potential massive amount of bioaccumulation of PFOS in the blood system are the cost of diseases. As shown in Figure 7, the United States is in the billions of dollars for medical expenses for several individual diseases per year. Some of these would include gastrointestinal diseases for over 100 billion dollars per year, cardiovascular diseases for an approximate of 219 billion dollars per year, and lung diseases for about 154 billion dollars per year [32, 61, 67]. The cost for diseases in the United States is very high and with further bioaccumulation of this contaminant, the cost can significantly increase due to higher health complications that can potentially arise from PFOS bioaccumulation.

Figure 7: Annual Disease costs in the United States

Economic impacts were also seen in form of corporate revenue losses from the two companies that started it all with the use of this toxic contaminant. As shown in Figure 8, the Minnesota Mining & Manufacturing Company lost an approximate of 850 million dollars in lawsuits for utilizing this toxic contaminant for so many years [44]. In a similar manner, the Dupont Company lost an approximate of 671 million dollars in lawsuit money [7]. Even though this is nothing compared to what these two companies made in revenue, they still lost their corporate money for the persistence use on PFOS production and utilization.

Figure 8: Corporate revenue losses for the long use of PFOS

1.5 PFOS and Fluorosulfonic acid description

The detailed structure and composition of PFOS can be observed in Figure 9. Structurally, PFOS is a molecule that is composed of a polar and non-polar end. This characterizes the molecule as unique due to the integrated polarity differences. The non-polar end of the molecule is composed of a total of 8 carbon atoms bonded to 17 fluorinated atoms. Due to the equal amount of electronegative pull that the fluorine atoms exert on the carbons, there is no net dipole moment for the water molecules to interact with. Therefore, the water molecules will have no interaction with this side of the molecule. However, the molecule also has a polar side to it composed of a sulfonic acid functional group. This means there is a total of 1 Sulfur atom double bonded to two oxygen atoms and single bonded to one alcohol group. The alcohol group that is composed of an oxygen atom single bonded to a hydrogen atom makes the sulfonic acid functional group of PFOS polar. This means the polar side of this molecule is very attracted to water and can bond strongly with water since there is an electronegative pull difference between the oxygen and the hydrogen. Due to the structural and polarity difference of both ends of the molecule, this project focuses more on the polar side of PFOS.

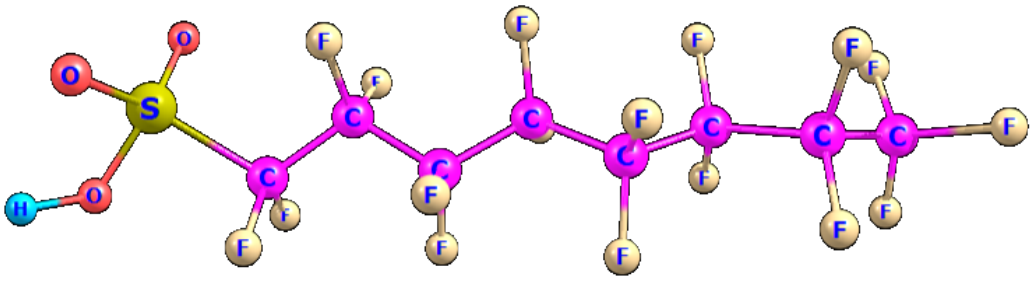

Figure 9: Detailed Chemical Structure and Composition of PFOS

1.6 Research Objectives

The University of Texas Rio Grande Valley mission statement is "To transform the Rio Grande Valley, the Americas, and the world through an innovative and accessible educational environment that promotes student success, research, creative works, health and well-being, community engagement, **sustainable development**, and commercialization of university discoveries." This project supports the UTRGV mission statement and aligns with the United Nations Sustainable Development goals. In order to achieve a more sustainable future for all, this project targets the challenges of the Life Below Water, the Good Health and Well-Being, and the Clean Water and Sanitation goals. The icons representing these United Nations Sustainable Development Goals can be seen in Figure 10. This project targets to increase the scientific knowledge to eventually develop research capacities to improve the ocean's health, to substantially reduce the number of deaths and illnesses from hazardous chemicals, and to improve the water quality by reducing the pollution and minimizing the release of hazardous chemicals [98].

Figure 10: The United Nations Sustainable Goals that this project targets.

This project has two phases to the objectives that revolve around this toxic environmental contaminant, PFOS. The first phase of the objective is composed creating a baseline for the environmental contaminants in a survey of along the coast of Putian city, located in southern China. This phase of the project is very important due to the limited amount of surveys being done in the southern part of China. For this portion of the research, there was a collaboration that

happened with the Putian Marine and Fishery Environment Monitoring Station in Fujian and the Marine Biotechnology Specialty located in Xiamen University Malaysia. Out of all the different contaminants that were surveyed, this project focused on reporting the locations at which the PFOS and other contaminants were exceeding the Chinese national standards.

The second part of the objective is composed of the examination of the structure and behavior of a shorter prototype molecule of PFOS, fluorosulfonic acid, as it interacts with water with high accuracy. This will be done by doing simulations of the first solvation shell of fluorosulfonic acid and then comparing the results to experimental analysis. The theoretical calculations and simulations will be done using Gaussian 16 carried out through the cluster computers at the Texas Advanced Computer Center (TACC) in Austin, Texas. The resulting calculations will be composed of the rotational constants and dipole moments of the molecules. This will let us know theoretically the molecule's structures and behavior as it solvates. The molecules that were studied theoretically involve the monomer of the fluorosulfonic acid, and the three complex hydrates. From the theoretical calculations, a rotational spectrum is simulated in order to compare it to the experimental section.

The experimental section is composed of studying the fluorosulfonic acid and its complex hydrates in a Fourier Transform Microwave Spectrometer. This instrument is used in order to prove the structure and behavior of the molecules in high accuracy. The monomer for fluorosulfonic acid will be studied in the University of Texas Rio Grande Valley's K-Broadband Chirped-Pulse Fourier Transform Microwave Spectrometer. For the study of the hydrate complexes, a collaboration with the University of Minnesota is necessary due to the lack of equipment. The University of Minnesota's Cavity-Based Fourier Transform Microwave Spectrometer is the instrumentation needed for the study of the all the hydrate complexes for

fluorosulfonic acid. Following the experimental section, the theoretical and experimental spectra will be fitted. The accurate fitting for the majority of the lines for both spectra will allow for the behavior of fluorosulfonic acid and its interaction with water to be proved.

CHAPTER II

ENVIRONMENTAL SURVEY ALONG THE COAST OF PUTIAN, CHINA

2.1 Introduction

Perfluorooctanoic Acid (PFOA) and perfluorooctanesulfonic Acid (PFOS) are types of perfluoroalkyl acids (PFAAs) that are composed of a nonpolar fluorinated carbon chain and a polar group of carboxylate or sulfonic acid [47, 58]. These stable compounds have unique properties such as being partially hydrophilic and lipophilic with low surface tension, low surface free energy, and high persistency to degradation [57, 102, 108]. These characteristics make PFOA and PFOS compounds very useful to the industry for a variety of commercial uses [9]. These applications include water and oil repellent, waxes, lubricants, firefighting foam, photolithography, and the production of coatings [102]. Since the early 1950s, PFAAs have been used for the production of these consumer products and consequently are released into the environment through waste, manufacturing, disposal, and degradation [42, 47, 58]. In 1999, The Environmental Protection Agency (EPA) ordered further examination on perfluorinated compounds upon rising concerns on possible identification of PFOA or PFOS found in the blood of humans and animals worldwide and the reported global spread toxicity [59]. In 2002 the leading manufacturing company in PFOS, the 3M Company, phased out on PFOS upon serious negotiation with the EPA [36, 99]. Shortly

after, in 2006, the EPA created the Stewardship Program in which eight major leading manufacturing companies agreed to phase out on PFOA and similar chemicals to stop the spread of the molecule's bioaccumulation and toxicity [36]. Several studies have hypothetically established strong possible correlations between people's exposure to PFAAs and the sharp growth of health problems in humans based on animal studies. It was found that possible exposures to high levels of PFAAs come from contaminated air, water systems, plants, and animals that serve as fundamental resources of life [58]. In addition, it is known that PFAAs such as PFOA remain in the human body for long periods [79]. In 2009 and 2019, the Stockholm convention listed PFOA and PFOS as emergent persistent organic pollutants (POPs) and they have been subjected to regulatory action and voluntary industrial phase-outs. In May 2019, more than 180 countries agreed to ban the production and use of PFOA, its salts, and PFOA-related compounds under the international Stockholm Convention on Persistent Organic Pollutants (POPs) [34].

Toxic pollutants such as heavy metals have been found in ocean waters and sediments worldwide due to their easy bioaccumulative and low degradative properties [30, 54]. Heavy metals are released into the environment naturally and anthropogenically. Hazardous heavy metals include Lead (Pb), Arsenic (As), Copper (Cu), Cadmium (Cd), Chromium (Cr), Aluminum (Al), Nickel (Ni), Zinc (Zn), and Manganese (Mn) (Jacob et al. 2018). Out of those heavy metals, the ones that are most commonly observed in water ecosystems are Cadmium (Cd), Copper (Cu), Zinc (Zn), Lead (Pb), Chromium (Cr), and Mercury (Hg) [62]. Heavy metals can enter the human body through various pathways including ingestion, inhalation, dermal contact, and consumption. [114] Irreversible harmful effects that heavy metals can have on the human body include the reduction of growth and organ development, the damage to the nervous system, the onset of cancer, and ultimately death. [62] Locations in which heavy metals have already been detected include parts

of the Pacific, Atlantic, and the Indian Ocean as well as several rivers, lakes, and other bodies of water around the world. [12, 89]

Recent studies have established the need for the regulation of PFAAs since PFAAs are found in ocean water all over the world. [36, 107] One study discussed the monitoring levels of PFOA samples in several regions of ocean water using a new analytical technique that allowed for higher sensitivity levels. The oceanic regions that were analyzed include the north and mid-Atlantic Ocean, central to the eastern Pacific Ocean, and other samples from specific regions of Asian countries such as Japan, China, and Korea. The water analysis was conducted using High-Performance Liquid Chromatography Mass Spectrometry (HPLC/MS). The analytical technique consisted of the replacement of the High-Performance Liquid Chromatography tubes to stainless steel polyetheretherketone tubes, the isolating of the Degasser and solvent-selection valves, the replacement of solvent inlet filters with stainless steel, higher amounts of water extraction samples, and the replacement of 10-g SPE Sepak® tC18 cartridges with Oasis® HLB cartridges. For this study, results showed that 80% of the ocean water samples contained PFOA and PFOS with PFOA being predominant with the range of 1800 to 192,000 pg/L followed by PFOS with a range of 338 to 57,700 pg/L. [107] Another related study involves the analysis of water from different ocean layers in the southern coastal area of Fujian Province. In total, there were 282 water samples collected that included a total of 94 sites and 19 different variable measurements such as temperature, pH, salinity, nutrients, oil, and heavy metals. The instrument used to analyze for detection of heavy metals was the atomic fluorescence spectrometer. Results showed that high levels of heavy metals were detected at a moderate level of salinity and that Zinc was the predominant metal found followed by copper, arsenic, lead, chromium (VI), Cadmium, and Mercury. [51]

In our study, the bodies of water near Putian city were analyzed to set a baseline on PFOA and PFOS as well as continuous monitoring of some heavy metal content. The areas that were analyzed in this research include Xinghua Bay, Pinghai Bay, Nanri Channel, Dongzheng Harbour, and Meizhou Bay. The city of Putian is located in the Fujian province in China and runs from 24°59'N to 25°46'N and 118°27'E to 119°56'E with a sea area of 11,0000 Km^2. [72] Neighboring the city, there is Fuqing City located northeast, Yongtai and Dehua located northwest, Nan'an City located southwest, and the Taiwan Strait located southeast. [52] Putian has been known to be an exportation base for the Fujian providence. The major bodies of water surrounding the city serve as the major source for industrial use, food source, and water supply. Due to the heavy water use by manufacturing companies, concerns have been raised over the possible negative impact on the surrounding environment, mainly contamination of water, air, and damage to the flora and fauna of the city. The contamination of the natural resources supplying the city may lead up to endangering and harming the people's health. [51]

2.2 Experimental Methods

The Solid Phase Extraction (SPE) Enrichment with Ultra-High-Performance Liquid Chromatography-Tandem Mass Spectrometry method developed by Huang *et al* [37] was used for the detections of PFOA and PFOS. The water samples were collected from 56 locations throughout Putian coastal region. The distribution of the collection sites is shown in Figure 11. The instrumentation used in the study include ultrasonic cleaner KQ3200E from Kunshan Ultrasonic, electronic balances (Sartorius BSA224S 0.0001g and Sartorius TE612-L 610g/0.01g), Rotary evaporator (Buchi R-210), Agilent 6410 Triple Quadrupole LC/MS, Mini-Q Direct8 water purification system, and C18 Solid Phase extraction Cartridges (500 mg/6 mL, BESEP, Beijing Zhenxiang). The seawater samples were collected and filtered through 0.45 μm glass fiber

membrane. The samples were then stored and sealed in glass containers and shipped to the laboratory. In the lab 0.5 mL of a 5.0 μg / L internal standard mixed solution was added to 500 mL of the filtered water sample. An activated C18 solid-phase extraction column was used for matrix separation and target enrichment at a flow rate of 5 mL/min. After the water samples have flowed through, the solid-phase extraction column is dried under vacuum for about 45 minutes, and then eluted with 15 mL of methanol-ethyl acetate mixed eluent (4:1). The effluent is collected and concentrated to near dryness. Methanol was then added to reach 1.0 mL volume for testing using Agilent 6410 Triple Quadrupole LC/MS. The stated limit of qualification (LOQ) is 0.5-1.5 ng/L.

For groundwater samples analysis, atomic absorption spectroscopy was used for the detections of Cu, Zn, Pb, and Cd (GB7475-87); cold vapor atomic fluorescence spectroscopy was used for the detections of Hg and As (HJ694-2014); Spectrophotometry was used for the detection of fluoride (HJ84-2016); Infrared spectrophotometry was used for petroleum compounds (HJ637-2012); the dichromate oxidation method was employed for the chemical oxygen demand (COD) (HJ828-2017); Nessler's reagent colorimetry was employed for ammonia nitrogen (HJ535_2009); alkaline potassium persulfate digestion-UV spectrophotometric method was employed for total nitrogen (HJ636-2012); and ammonium molybdate spectrophotometry was used for total phosphorus (GB11893-1989). The results will be discussed with regard to Environmental Quality Standards for Surface Water (GB3838-2002).

For the analysis of seawater samples, atomic absorption spectroscopy was used for the detections of Pb, Cd, and Cu (except for samples from Xinghua Bay which were treated with ICP-MS) [38]; cold vapor atomic fluorescence spectroscopy was used for the detection of As (Xinghua Bay samples were also treated with ICP-MS) [38]; cold vapor atomic fluorescence spectroscopy was used for the detection of Hg; Spectrophotometry was used for the detections of nitrogen and

phosphorus; the potassium permanganate oxidation method was employed for the detection of COD and UV-visible spectrophotometry was used for the detection of petroleum compounds. All of the above methods, except for ICP-MS, were carried out following the protocols described in source GB 17378.4-2007. The results will be discussed with regard to Seawater quality standard (GB3097-1997).

The above instruments from Putian Marine and Fishery Environment Monitoring Station were used for data analysis. Water samples were collected from 56 locations around Putian city and its surrounding areas (Figure 11) in January 2019.

2.3 Results and Discussion

2.3.1 Levels of PFOA and PFOS in Putian Coastal Region:

Putian has become an export base for Fujian products. The main industries are shoe-making, brewing, electronics, garments, and machinery and electrical goods. There have been concerns regarding the increasing chemical contamination to surface water due to rapid industrial development and the lack of effective chemical control and waste management. The water bodies are used for irrigation in agriculture and also serve as sources of drinking water. The present study was initiated to investigate the PFOA and PFOS levels in water from various locations in Putian. The data collected in our experiments show low levels of PFOA and PFOS in most of the areas that were surveyed, suggesting that urban discharge may not be an important source of PFOA and PFOS in Putian area. The instrumentation used had a higher level of detection compared to the concentrations of PFOS and PFOA found in seawater and groundwater. Only one area located in Sanjiangkou was detected with a concentration of 99.4 ng/L for PFOA, and two areas in Sanjiangkou and Jiangkou bridge were detected with the approximated calculated concentrations

of 127 and 144 ng/L, for PFOS. Sanjiangkou is located at the end of Mulan Creek and Jiangkou bridge is located near the ocean entrance of Qiulu Creek. There have not been established standard for PFOA and PFOS in groundwater. For reference, the safety standard lifetime exposure for PFOA and PFOS in 70 ng/L for drinking water according to the U.S. Environmental Protection Agency. It would be interesting to compare our results to the samples from Jiulongjiang in nearby city of Xiamen reported by Huang *et al.* [37] PFOA and PFOS were detected in all nine samples with averaged concentrations of 2.14 ng/L and 4.92 ng/L, respectively. The difference may be attributed to the much larger river runoff of Jiulongjiang River comparing to the creeks in Putian. And the more industrial and residential activities along Jiulongjiang River.

2.3.2 Other chemicals that fall within the standard:

Petroleum compounds and all heavy metal levels in surface water samples were below category I as set by the Chinese Environmental Quality Standards for Surface Water (GB-3838, 2002) for all the tested areas. The petroleum compounds were compared to the oil standard concentrations, and the heavy metals, including copper (Cu), Zinc (Zn), Cadmium (Cd), Lead (Pb), Mercury (Hg), and Arsenic (As), were compared to the standards shown supplemental files. This means that for these compounds, the quality of water is acceptable in all tested areas located North-West from the Meizhou Bay area and South-West from Xinghua Bay. As far as other chemicals being surveyed in groundwater, some were exceeding the standards in some locations while others were within the standards in other locations. The rest of the chemicals monitored include ammonia nitrogen, total nitrogen, total phosphorus, fluoride, and the chemical oxygen demand (COD). For Fluoride, all the locations were within category III for the surface water standard of 1.0 mg/L as shown in supplemental files. This indicates that the water for all the locations tested within the city North-West from Meizhou Bay and South-West of Xinghua Bay could not possibly be categorized

as polluted or severely polluted. However, they could be categorized under either excellent, good, or slightly polluted depending on the standards for the first two categories. For the ammonia nitrogen concentration, the standard for surface water is 0.15 mg/L for excellent quality of water, 0.5 mg/L for good quality of water, 1.0 mg/L for slightly polluted water, and 1.5 mg/L for polluted water, and 2.0 mg/L for severely polluted water. The data obtained for ammonia nitrogen show that in two locations, Jiangge Dam and Dongzheng Dam, the water is within the standard for the classification I for surface water quality of 0.15 mg/L. This indicates that in these two locations, Jiangge Dam located in the reservoir of water on the upper stream of the Mulan River and Dongzheng Dam that passes through the Yanshou River, the water quality can be categorized as excellent. In the Xitai Bridge located in the entrance of Daji River from the division of the Mulan River and Laixi Creek around the Laixi Clinic along the Mulan River, the concentrations for ammonia nitrogen exceed the class I category of 0.15 mg/L but are within the class II category of 0.5 mg/L. This shows that in these locations, the water is still classified as of good quality. For COD, several locations were within class III levels of 20 mg/. The locations include Jiangge Dam, Xitai Bridge, and Shima Bridge which is located along the Mulan River North-West of the Meizhou Bay. It also includes Yuantou Bridge located near Zhanglin Bridge and its intersection with Hualin Rd, Laixi Creek, Dongzheng Dam, and Jiangkou Bridge which is located in the entrance of the Qiulu River from the Xinghua Bay. This means that the quality of water could fall under either excellent, good, or slightly polluted quality of water based on the standards of the first two categories. For total nitrogen (TN), only 2 locations were under the standards for class III of 1 mg/L. These two locations include Jiangge Dam and Dongzheng Dam, and could possibly fall under either excellent, good, or slightly polluted quality of water depending on the standards for the first two categories. For total phosphorus (TP), only two locations, Jiangge Dam and

Dongzheng Dam, were within the standard of class III of 0.05 mg/L. This indicates that in these two water locations, the water quality could fall under either excellent, good, or slightly polluted quality of water depending on the standards of the first two categories.

In the collected samples of seawater, several chemicals were within the category I levels for Seawater Quality Standards of China (GB 3097, 1997) in all the tested areas (Table 3). These chemicals include COD, copper (Cu), Lead (Pb), and arsenic (As). This means that for all these chemicals, the concentrations of these ions are within acceptable levels in all the tested locations around the Xianghua, Meizhou, and Pinghai Bay indicating the water is clean and fit for human consumption. For the rest of the chemicals tested, we found least one location in which the concentrations were exceeding category I of clean water. The rest of the chemicals analyzed for in seawater include inorganic nitrogen, inorganic phosphorus, oil, Cadmium (Cd), and mercury (Hg). For inorganic nitrogen, the locations that were within the standards include all Pinghai Bay areas (pH), and all Meizhou Bay areas (MZ) located South-East of Putian city. All these water locations had inorganic nitrogen concentrations within Category I of 0.20 mg/L and are therefore categorized under clean water. Another area that could still be categorized as relatively clean water for inorganic nitrogen, is in XH07. In this location, the inorganic nitrogen concentration exceeded category I of 0.20 mg/L but not category II of 0.30 mg/L. For inorganic phosphorus, the measured concentrations were compared to those of Phosphate concentrations. The locations pH1 to pH6, MZ10 to MZ12, MZ15 to MZ17, XH14, and XH19 were all under the category I standard of 0.015 mg/L and are categorized under the clean water category. Other areas that are categorized under the relatively clean water standard are pH7, MZ01 to MZ09, MZ13, XH08, and XH15, to XH17. This is due to the concentrations for total phosphorus exceeding category I of 0.015 mg/L, but not exceeding category II of 0.030 mg/L. For oil, all locations were under the category I standard of

0.05 mg/L except for the location XH06. This means that for all the locations, with the exception of XH06, the water is categorized as clean water. For the XH06 location, the concentration for oil was detected to be 80 μg/L. It should be noted that the standard for clean water is 0.05 mg/L, or 50 μg/L and that the standard for relatively clean water is 0.3 mg/L, or 300 μg/L. This means that in this area, even though category I was exceeded, the concentration of oil was still within category II and the water for this location can be categorized as relatively clean water. For Cadmium, all the areas were within the standard for category I for seawater quality of 0.001 mg/L or 1 μg/L with the exception of the location MZ08. This means that the water is categorized as clean with the exception of MZ08. For the area MZ08, the concentration is 1.32 μg/L, which exceeds category I of 1 μg/L, but is within the category II standard of 0.005 mg/L or 5 μg/L. This data indicates that for this location, the water is still categorized as relatively clean water. For Mercury (Hg), the locations pH1 to pH7, MZ01 to MZ05, MZ08, MZ10 to MZ12, XH06, XH08, XH10, XH12, and XH15 to XH19 were all under the category I standard of 0.00005 mg/L or 0.05 μg/L and also categorized as clean water. Other concentrations that still fall under the relatively clean water category include XH01, to XH05, XH07, XH09, XH11, and HX14. This is because the concentrations for Mercury (Hg) exceed category I standard of 0.05 μg/L but are within the category II standard of 0.0002 mg/L, or 0.2 μg/L. Based on these results these locations are can be categorized as having relatively clean water.

2.3.3 Significant Pollutant concentrations

Notable concentrations of ammonia nitrogen in groundwater can be seen in the locations of Sanjiangkou, Shima Bridge, Yuantou Bridge, and Jiangkou Bridge located closest to the Xinghua and Meizhou Bays. In the locations of Shima Bridge, Yuantou Bridge, and Jiangkou

Bridge, the concentrations exceed category II for the surface water standard of 0.5 mg/L. Based on these results the quality of water can be categorized as slightly polluted in these locations. The remaining location, Sanjiangkou, exceeds category III of 1.0 mg/L. This indicates that the quality of water in this location can be categorized as polluted water. For COD, only two locations were observed to have notable significance. The area in which the highest concentration was observed was in Sanjiangkou located very close to the Xinghua Bay area. Samples from this area showed a concentration exceeding class III of 20 mg/L, but not exceeding class IV of 30 mg/L. This indicates that the water in Sanjiangkou can be categorized as polluted water. The other high concentration can be seen in Jiangkou Bridge, also very near the Xinghua Bay area, that is close to exceeding the class III standard of 20 mg/L. Therefore, the water of this area can be categorized under the slightly polluted. For total nitrogen (TN), the most significant concentrations were found in Xitai Bridge, Shima Bridge, Yuantou Bridge, Laixi Creek, Sanjiangkou, and Jiangkou Bridge. These locations exceed the class V standard of 2 mg/L. This indicates that these locations are beyond severely polluted water and require immediate attention for water treatment. Another notable concentration can be seen in Dongzheng Dam, where the concentration reported is close to exceeding class III of 1 mg/L and therefore categorized as slightly polluted water. For total phosphorus (TP), there were several regions in which classifications IV and V were being exceeded. These areas include Xitai Bridge, Shima Bridge, Yuantou Bridge, Laixi Creek, Snajiangkou, and Jiankou Bridge. Out of these locations, the one that needs the most attention for water treatment is Sanjiangkou. In this location, the total phosphorous concentration exceeds class V of 0.2 mg/L. This means that the water in this area is beyond severely polluted with phosphorus and needs immediate attention. Other high phosphorous concentrations were observed in Xitai Bridge, Shima Bridge, Yuantou Bridge, Laixi Creek, and Jiankou Bridge. In these locations, the

concentrations for total phosphorus exceeded that of class IV standards of 0.1 mg/L but do not exceed class V of 0.2 mg/L. This reveals that the water in these locations should be categorized as severe polluted water.

High concentrations of inorganic nitrogen and phosphorous in seawater were detected in several locations. For inorganic nitrogen there were several locations exceeding the Chinese Standards in Xinghua Bay (XH locations). The locations needing more attention include XH01, XH02, XH04, XH09, XH10, XH11, XH12, XH14, and XH16. These areas are the borderline areas in the upper part of Xinghua Bay that exceed the Chinese Seawater standard for inorganic nitrogen for medium polluted water of 0.50 mg/L. It is indicated that these areas are heavily polluted and require immediate attention for water treatment. Other areas that also require attention are in XH05, XH06, XH15, XH17, and XH19. These areas are located more towards the opening end of the Xinghua Bay and the concentrations inorganic nitrogen exceed the slightly polluted water category of 0.40 mg/L but fall within the medium polluted water standards of 0.50 mg/L. This means that all these areas can be categorized has having a medium polluted water quality. Other notable areas include XH03 and XH08 that exceed the seawater standard for relative clean water of 0.30 mg/L but fall within the Slightly polluted water category of 0.40 mg/L. This indicates that these water areas are categorized as slightly polluted water. For inorganic phosphorus, the concentrations were compared to the phosphate concentrations. The locations where most attention for water treatment is needed are in XH01, XH02, XH04, XH11, XH12. These locations are once again border-lining the Xinghua Bay and the concentrations for inorganic phosphorus exceed the standard of 0.045 mg/L of medium polluted water. This indicates that in these locations the water can be categorized under heavily polluted water. Other notable areas that exceed the relatively clean water standard of 0.030 mg/L but fall within the slightly polluted water category of 0.045

mg/L are XH03, XH05, XH06, XH07, XH09, XH10. Based on these data, the water in these regions can be ~~is~~ categorized as slightly polluted water.

2.4 Conclusion

An environmental contaminant survey was conducted in several bodies of water near Southern China, Putian City. Both seawater and groundwater were tested for heavy metals, PFOS, PFOA, COD, Inorganic nitrogen, Inorganic phosphorus, Fluorides, oil, and petroleum compounds. The water analysis was performed by using High-Performance Liquid Chromatography Mass Spectrometry (HPLC/MS). Spectroscopic methods included atomic absorption, cold vapor atomic fluorescence and infrared. This is the first investigation of the PFOA and PFOS contaminations in water in Putian area. In all of the areas tested, PFOA and PFOS were not detected by our methods in most of the samples. These results established the baseline for this area. The emission of toxic chemicals including PFOA and PFOS into the environment should be continuously monitored. For groundwater and seawater, most of the contaminants were within the range established by the Chinese Environmental Quality Standard for Surface Water (GB 3838) and the Chinese Seawater Quality Standard (GB 3097). However, the contaminants that do need attention for water treatment in at least one or more tested areas for groundwater include COD, ammonia nitrogen, total nitrogen, and total phosphorus. Similarly, for seawater, the contaminants that need more attention, in at least one or more areas, include inorganic nitrogen and inorganic phosphorus.

2.4.1 Supplementary materials

See supplementary material for the contamination standards of China on various chemicals in Appendix A.

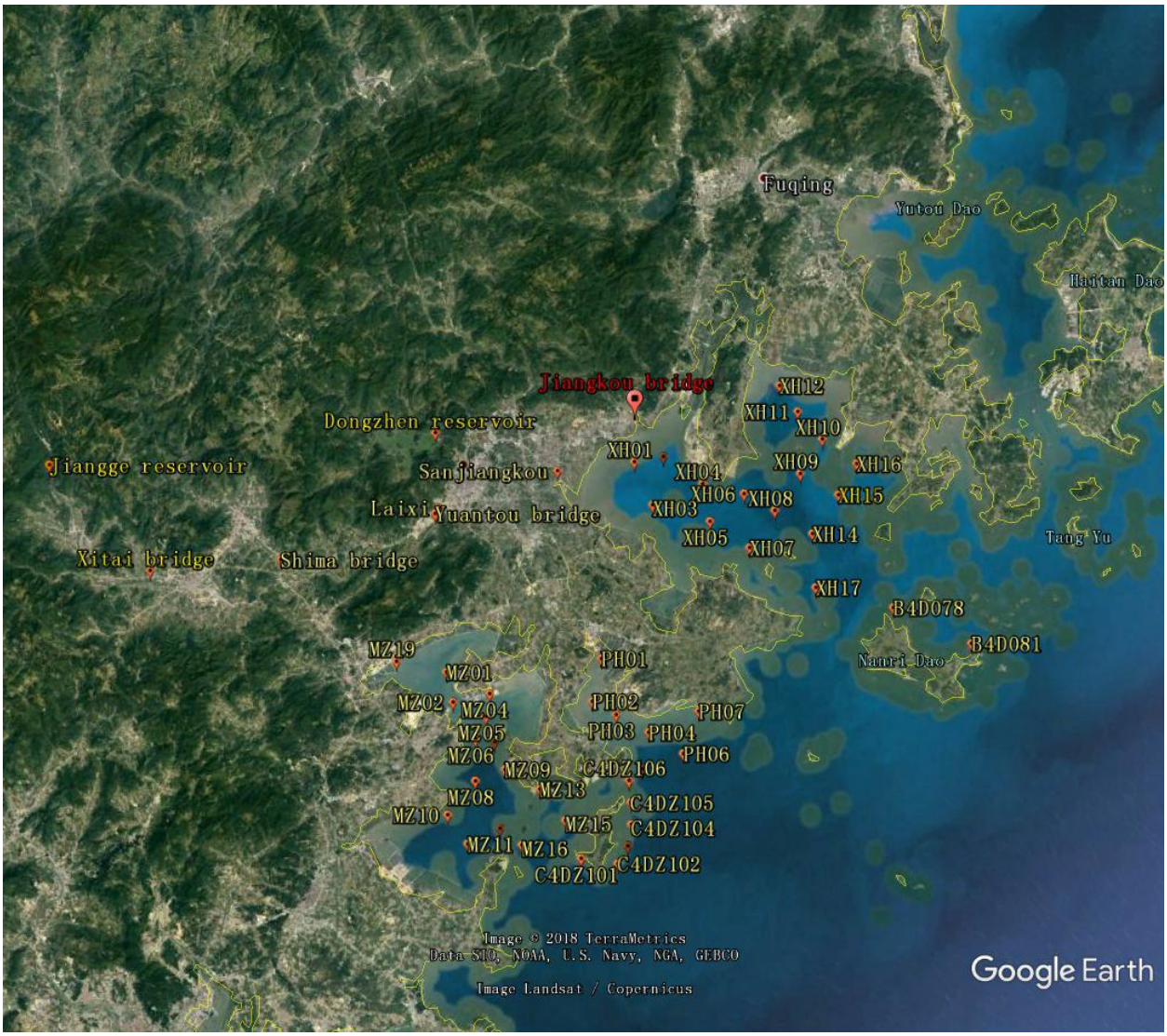

Figure 11 Locations of 56 sampling sites along the Putian coastal region as well as the surrounding rivers.

Table 1 Locations of all sampling along Putian Coastal regions and surrounding rivers

Xinghua Bay	East Longitude	North Latitude
XH01	**119°12'03”**	**25°25'45”**
XH02	**119°14'04”**	**25°25'54”**
XH03	**119°13'00”**	**25°23'00”**
XH04	**119°16'32”**	**25°23'59”**
XH05	**119°16'46”**	**25°21'39”**
XH06	**119°19'17”**	**25°23'08”**
XH07	**119°19'16”**	**25°19'48”**

XH08	**119°21'15”**	**25°21'55”**
XH09	**119°23'15”**	**25°24'01”**
XH10	**119°25'00”**	**25°26'00”**
XH11	**119°23'32”**	**25°27'51”**
XH12	**119°22'29”**	**25°29'34”**
XH14	**119°23'38”**	**25°20'16”**
XH15	**119°25'41”**	**25°22'29”**
XH16	**119°27'09"**	**25°24'17"**
XH17	**119°23'28”**	**25°16'58”**
XH19	**119°26'52”**	**25°19'32”**

Nanri Island	East Longitude	North Latitude
B4D081	**119°33'32.9”**	**25°12'36.6”**
B4D078	**119°28'33.3”**	**25°15'16.1”**

Meizhou Island	East Longitude	North Latitude
C4DZ101	**119°05'50”**	**25°02'03”**
C4DZ102	**119°08'15”**	**25°01'31”**
C4DZ103	**119°09'02”**	**25°02'31”**
C4DZ104	**119°09'25”**	**25°03'47”**
C4DZ105	**119°09'31”**	**25°05'06”**
C4DZ106	**119°09'33”**	**25°06'26”**

Pinghai Bay	East Longitude	North Latitude
PH01	**119°08'30.2”**	**25°13'57.3”**
PH02	**119°07'36.8”**	**25°11'25.2”**
PH03	**119°09'7.2”**	**25°10'28.7”**
PH04	**119°11'11.0”**	**25°09'12.8”**
PH05	**119°10'30.4”**	**25°07'02.9”**
PH06	**119°13'22.2”**	**25°07'43.7”**
PH07	**119°14'41.6”**	**25°10'11.0”**

Along the Mulan Creek	East Longitude	North Latitude
Jiangge Dam	**118°32'21.08”**	**25°29'0.06”**
Xitai Bridge	**118°38'33.28”**	**25°21'57.91”**
Shima Bridge	**118°47'27.94”**	**25°21'52.06”**
Yuantou Bridge	**118°58'12.13”**	**25°23'46.23”**
Laixi Creek	**118°58'26.38”**	**25°24'7.11”**
Jiangkou Bridge	**119°12'26.18”**	**25°28'59.04”**

Sanjiankou	**119°6'46.18”**	**25°25'40.11”**
Dongzheng Dam	**118°58'42.93”**	**25°28'44.60”**

Meizhou Bay	East Longitude	North Latitude
MZ01	**118°57'59”**	**25°14'03”**
MZ02	**118°58'14”**	**25°12'12”**
MZ04	**119°00'45”**	**25°12'30”**
MZ05	**119°00'22”**	**25°11'08”**
MZ06	**118°59'31”**	**25°09'50”**
MZ07	**119°00'47”**	**25°09'33”**
MZ08	**119°59'15”**	**25°07'19”**
MZ09	**119°01'18”**	**25°07'50”**
MZ10	**118°57'11”**	**25°05'27”**
MZ11	**118°58'21”**	**25°03'35”**
MZ12	**119°00'36”**	**25°04'20”**
MZ13	**119°03'31”**	**25°06'27”**
MZ15	**119°05'02”**	**25°04'25”**
MZ16	**119°01'58”**	**25°03'12”**
MZ17	**119°04'39”**	**25°02'56"**
MZ19	**118°54'41”**	**25°15'00”**

Table 2: Concentrations of groundwater samples (unit: μg/L for heavy metals and mg/L for others)

	Jiangge Dam	Xitai Bridge	Shima Bridge	Yuantou Bridge	Laixi Creek	Sanjiangkou	Jiangkou Bridge	Dongzhen Dam
Ammonia nitrogen	0.06	0.26	0.63	0.54	0.42	1.14	0.61	0.087
Total nitrogen	0.78	2.92	3.36	3.35	3.17	4.38	2.97	0.938
Total phosphous	0.02	0.16	0.16	0.18	0.15	0.25	0.14	0.02
COD	4	8	11	10	11	25	19	9.3
Fluoride	0.136	0.177	0.194	0.171	0.194	0.294	0.261	0.074
Petroleum compounds	0.01	0.02	0.02	0.02	0.03	0.03	0.02	0.01
Cu	0.42	0.74	0.97	2.11	1.06	2.04	5.02	0.08
Zn	8.6	8.6	9.6	10.8	9.1	10.0	10.5	0.7

Cd	0.05	0.05	0.05	0.05	0.05	0.05	0.05	0.05
Pb	1.81	1.73	1.78	1.70	1.70	1.90	1.72	0.21
Hg	0.04	0.04	0.04	0.04	0.04	0.04	0.04	0.04
As	0.3	0.5	0.8	0.9	0.9	1.4	0.5	0.3

Table 3: Concentrations of seawater samples (unit: μg/L for oil and heavy metals, and mg/L for others)

	Inorganic Nitrogen:	Inorganic Phosphorous:	COD:	oil:	Cu:	Pb:	Cd:	Hg:	As:
pH1:	0.127	0.0147	0.39	21.4	0.84	0.19	0.039	0.016	1.68
pH2:	0.117	0.0146	0.29	24.3	1.03	0.17	0.054	0.016	1.65
PH3:	0.107	0.012	0.26	21.6	0.81	0.15	0.042	0.016	1.4
pH4:	0.126	0.0115	0.11	26.4	1.98	0.15	0.057	0.015	1.33
pH5:	0.085	0.01	0.28	24	1.19	0.23	0.086	0.02	0.9
pH6:	0.093	0.0118	0.34	39.9	1.23	0.19	0.052	0.013	1.39
pH7:	0.1	0.0292	0.14	44.4	1.17	0.17	0.042	0.015	1.6
MZ01:	0.17	0.026	0.49	14	1.04	0.24	0.26	0.005	1.34
MZ02:	0.172	0.028	0.45	11	0.93	0.23	0.32	0.004	1.38
MZ04:	0.156	0.022	0.69	12	1.21	0.32	0.36	0.005	1.33
MZ05:	0.149	0.021	0.45	7	1.07	0.27	0.27	0.002	1.32
MZ06:	0.155	0.027	0.51	12	1.32	0.36	0.38		1.33
MZ07:	0.158	0.021	0.65	10	1.09	0.31	0.38		1.3
MZ08:	0.128	0.018	0.47	10	0.01	0.29	1.32	0.004	1.32
MZ09:	0.149	0.02	0.61	8	4.47	0.4	0.31		1.29
MZ10:	0.084	0.014	0.49	8	0.94	0.27	0.33	0.002	1.33
MZ11:	0.106	0.014	0.47	8	0.82	0.3	0.37	0.002	1.33
MZ12:	0.066	0.012	0.41	7	4.47	0.31	0.27	0.002	1.3
MZ13:	0.11	0.017	0.53	7	0.94	0.3	0.27		1.26
MZ15:	0.085	0.014	0.49	7	0.8	0.24	0.36		1.32
MZ16:	0.065	0.011	0.37	7	0.76	0.29	0.2		1.29
MZ17:	0.092	0.014	0.45	7	0.82	0.24	0.32		1.26
XH01:	0.702	0.068	0.55	36	3.21	0.34	0.22	0.11	2.2
XH02:	0.598	0.063	0.51	26	3.9	0.41	0.26	0.11	2
XH03:	0.354	0.04	0.78	26	2.58	0.44	0.14	0.057	2.3
XH04:	0.76	0.064	0.66	24	3.26	0.3	0.27	0.09	1.9
XH05:	0.44	0.038	0.81	38	2.97	0.76	0.14	0.08	2.2

Table 3: Continued concentrations of seawater samples (unit: μg/L for oil and heavy metals, and mg/L for others)

XH06:	0.46	0.033	0.57	80	3.63	0.24	0.12	0.045	2.2
XH07:	0.29	0.033	0.84	27	2.63	0.62	0.18	0.066	3.2
XH08:	0.34	0.026	0.6	45	3.44	0.68	0.2	0.17	1.9
XH09:	0.68	0.03	0.69	20	3.56	0.82	0.15	0.064	1.9
XH10:	0.67	0.032	0.48	30	3.32	0.28	0.08	0.016	2.4
XH11:	0.88	0.052	0.59	24	3.27	0.27	0.14	0.059	2.5
XH12:	0.93	0.06	0.6	18	3.29	0.44	0.23	0.011	2.9
XH14:	0.63	0.015	0.54	14	2.31	0.69	0.19	0.051	2.6
XH15:	0.47	0.019	0.52	25	2	0.29	0.08	0.012	2.2
XH16:	0.54	0.016	0.4	20	1.94	0.35	0.1	0.011	2.1
XH17:	0.43	0.017	0.48	16	2.18	0.28	0.11	0.032	2.1
XH19:	0.4	0.014	0.47	18	1.99	0.19	0.07	0.008	2.6

CHAPTER III

ROTATIONAL SPECTROSCOPY

3.1 Introduction to Rotational Spectroscopy

Rotational spectroscopy, also known as microwave spectroscopy, is a technique that can help identify precise values that define a molecule's detailed structure and identity. Characteristics such as the molecule's bond lengths, angles, number of conformers, and dissociation energies can be obtained with high accuracy. [2, 105] In microwave spectroscopy, microwave radiation is used to provide the molecule with enough energy to make it rotate. As seen in Figure 12, the radiation used to observe the rotational transitions is in a range from a wavelength of 10^3 μm to more than 10^6 μm, or from a strength of approximately 300 MHz to 300 GHz. [84]

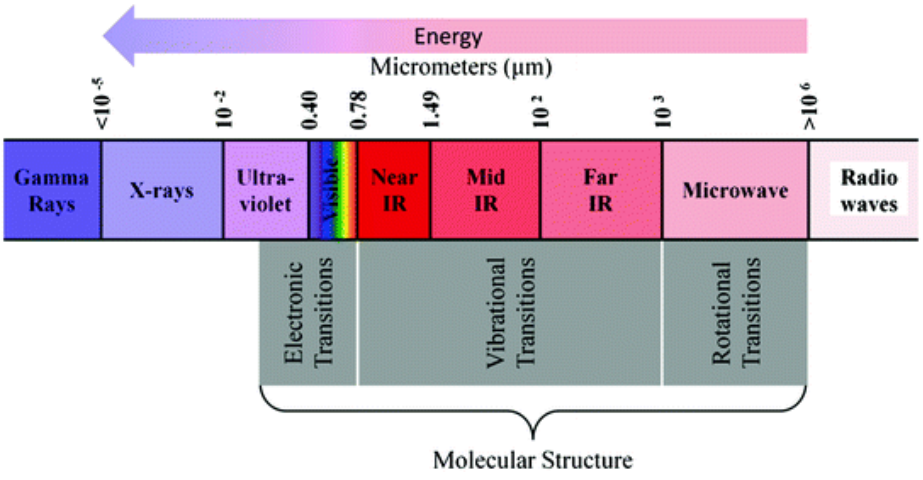

Figure 12: Electromagnetic Spectrum

After the molecule uses that energy and the rotations come to an end, the molecule emits the energy into the environment. That energy gets picked up by the microwave spectrometer to then convert it into a spectrum. The Fourier transform will help in converting the emitted signals from a time-domain scenario to a frequency domain spectrum. [53]

Rotational spectroscopy has 2 main criteria for the technique to work. The first one is that in order to analyze a molecule, the chemical must be in a gaseous phase. That is because the molecule must be in a free chemical environment in order to be able to interact fully with the radiation and be able to absorb the maximum energy possible. The second requirement is that the molecule must have a dipole moment to be able to interact with electromagnetic field and have measurable energies from the rotational transitions. [5, 10, 65] Since we are talking about the rotational system of a molecule, everything we know in terms of linear systems must be changed into terms of rotational systems. Table 4 shows the conversions from describing a linear motion system to an angular motion system. It is very important to get familiarized with the angular motion system, since in this thesis the discussions will be in terms of angular motion.

Table 4: Relationship between and Angular and Linear Motion

Linear Motion	"Property"	Angular Motion
Distance, x	Position	Angle, θ
Velocity, $v = \frac{dx}{dt}$	Velocity	Angular Velocity, $\omega = \frac{d\theta}{dt}$
Acceleration, $a = \frac{d^2x}{dt^2}$	Acceleration	Angular Acceleration, $\alpha = \frac{d^2\theta}{dt^2}$
Mass, m	Mass	Moment of Inertia, $I = mr^2$
Linear Momentum, $p = mv$	Momentum	Angular Momentum $L = I\omega$
Kinetic Energy, $E_k = \frac{1}{2}m\,v^2$	Kinetic Energy	$E_k = \frac{1}{2}I\omega^2 = \frac{L^2}{2I}$

The best way to start introducing rotational spectroscopy constants and equations, would be to discuss the theory behind the rotary motion of the simplest molecule in terms of its geometry. That would be a rigid linear or diatomic molecule rotating in free space. [59, 94] When looking at a diatomic molecule, you have a simple geometric structure with all atoms passing through one main axis. Because there is only one main fixed axis to look at, is that only one rotational constant, B, is used to describe the rotary movement of the molecule. When the molecule gets more complex in terms of geometry and symmetry, it can utilize all 3-dimensional axis, and therefore have 2 other additional rotational constants, A & C to help describe the rotary motion of the molecule.

In rotational spectroscopy, molecules can be categorized within five different classifications based of their geometric structures and the rotational constants. When discussing the rotary motion of a molecule, the rotational constants are the values that are the bridge between the moment of inertia, the bond lengths of the molecules, and the difference in energies from the rotational transitions of the spectra. Table 5 shows all the classifications and the rotational constants that classified within the geometry.

Table 5: Categories of different geometric structures

Linear/Diatomic Molecule		B = C, A=0
Spherical Top		A = B = C
Symmetric Top	Prolate	A > B = C
	Oblate	A = B > C
Asymmetric Top		A > B > C

The type of molecule that will be discussed in this research, fluorosulfonic acid, follows the asymmetric top category. However, for the basic understanding of the theory behind the asymmetric top category, I will start with an example of a diatomic molecule.

3.2 Rigid Rotor & Diatomic/Linear Molecules

A diatomic molecule consists of a linear molecule composed of two atoms with a fixed distance as shown in Figure 13.

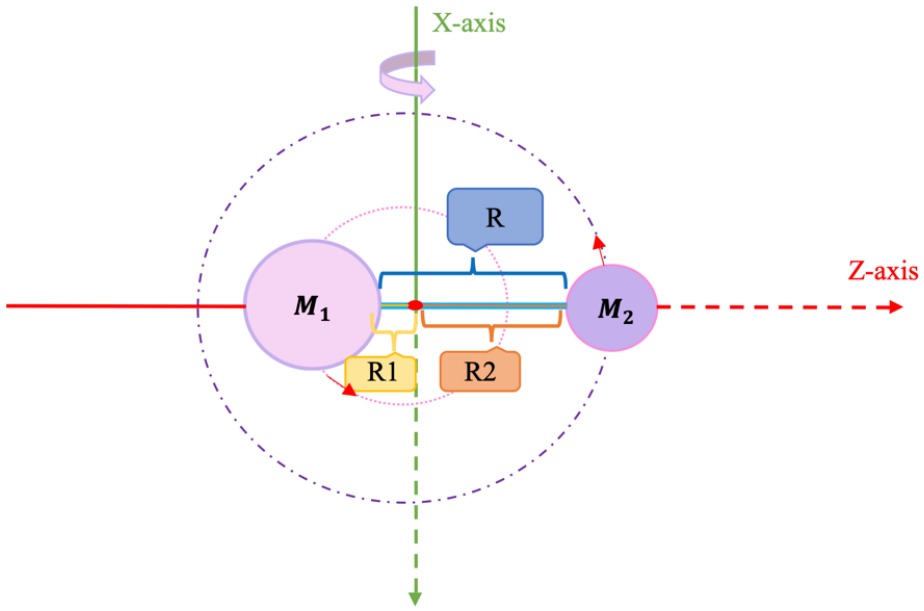

Figure 13: Rigid Rotor Model

In this model, known as the rigid rotor, we have two different atoms with unequal masses bonded by a stiff and rigid bond. The masses also unequal distances to the axis of rotation passing through the center of mass symbolized by a small red circle. It can be noted that the figure is not in the typical cartesian coordinate system, but the principal axis system. In this system the axis that is passing through both molecules is set to be the z-axis because it is the most important axis of symmetry. To best represent this figure in terms of rotation, the a, b, c-principal axis system is used. This is because the a, b, c-principal axis system rotates

together with the molecule and takes into account the moments of inertia I_x, I_y, and I_z or I_a, I_b, and I_c. This labeling scheme depends upon the inequality $I_c \geq I_b \geq I_a$ to hold. For a planar molecule, such as a diatomic molecule, the moment of inertia going out from the plane should be equal to the sum of the other two. [5]

In order to start talking about the energy for this simple model, we need to first talk about quantum mechanics. Quantum mechanics is a set of laws and concepts that help describe the motion of particles at the atomic and subatomic level. When talking about spectroscopy in the rotational phase, the application of the time-independent Schrödinger's equation from quantum mechanics helps explain the energy and detailed information of a system. The time-independent Schrödinger's equation can be written in an operator form such as

$$\hat{H}\psi = E\psi \tag{3.1}$$

This equation is quite complex on its own and contains several variables about a molecule's information. The Hamiltonia operator, $\hat{H}$, resembles with the total energy of a molecule, including kinetic and potential energy. The symbol ψ is a wavefunction that represents the dynamical information of the system such as its position and momentum.

The general expression for energy in classical mechanics for a rigid rotor is

$$E_k = \frac{1}{2} I\omega^2 \tag{3.2}$$

This equation is only composed of the kinetic energy in the Hamiltonian because the molecule is always in motion. Therefore, the potential energy is excluded from this equation. [11] The symbol I would be moment of inertia and the ω the angular velocity. The general expression for the moment of inertia would be

$$I = \sum_i m_i r_i^2 \tag{3.3}$$

where the equation takes into consideration the mass of the atom and the perpendicular distance from that of the rotary axis. For the rigid rotor, the complete expression would take into consideration the motion only in the x- and y- coordinates as shown below.

$$E_k = \frac{1}{2} I_x \omega_x^2 + \frac{1}{2} I_y \omega_y^2 \tag{3.4}$$

The z-component of the equation is excluded due to a 0 moment of inertia in the z-axis. This is because all the atoms are placed within the z-axis and there aren't any atoms positioned perpendicular to the center of rotation. The expressions describing the system result in $I_x = I_y$ and $I_z = 0$. [1] Therefore, for this scenario $x = c,\ y = b$, and $z = a$. Another way in which it can be written would be $I_b = I_c$ and $I_a = 0$. This resembles with table 5 since the rotational constant A, B, and C have an inversely proportional relationship to I_a, I_b, and I_c. Therefore, $I_b = I_c$ and $I_a = 0$ can be written as $B = C$, and $A = 0$.

For the rigid rotor, the moment of inertia for I_b or I_c is then equal to

$$I = \mu R^2 \tag{3.5}$$

Where

$$\mu = \frac{m_1 m_2}{m_1 + m_2} \quad \& \quad R = r_1 + r_2 \tag{3.5, 3.6}$$

This is because the equation is written based on a one-body problem instead of a two-body system. [59] Therefore, it takes the system into consideration from the point of view from the center of mass and the center of axis of rotation.

From the classical mechanics equation in 3.2, the kinetic energy for a rigid rotor can be rewritten to

$$E_k = \frac{L^2}{2I} \tag{3.7}$$

by rewriting $E_k = \frac{1}{2} I\omega^2$ to $E_k = \frac{1}{2} \frac{I^2\omega^2}{I}$ and then substituting L for $I\omega$. Now the equation will be in terms of the angular momentum, L, the moment of inertia. Then, from equation 3.7, the angular momentum can be replaced by symbol $\hat{J}$, that indicates the total angular momentum in quantum mechanics. This makes the equation of classical mechanics shown in equation 3.8 translated to the Hamiltonian of quantum mechanics.

$$\hat{H} = E_k = \frac{\hat{J}^2}{2I} \tag{3.8}$$

The solution to the time-independent Schrödinger's equation once this Hamiltonian is plugged in, is then solved with the help of the eigenfunction of the rigid rotor, the spherical harmonics, where

$$\hat{J}^2\psi_{l,m} = \hbar^2 J(J+1)\psi_{l,m} \tag{3.9}$$

And the eigenvalue is solved to be

$$E = \frac{\hbar^2}{2I} J(J+1) \tag{3.10}$$

Now, having gotten to this point is that we can properly introduce the rotational constant, B, that is equal to

$$B = \frac{\hbar^2}{2I} \tag{3.11}$$

So that equation 3.10 simplifies to

$$E = BJ(J+1) \tag{3.12}$$

This equation helps to note easier the fact that the energies are quantized in terms of $\hbar$. According to the selection rules for diatomic/linear molecules, $\Delta J = \pm 1$. [6, 95, 104] The energy diagram for the selection rules referring to the rigid rotor can be seen in Figure 14.

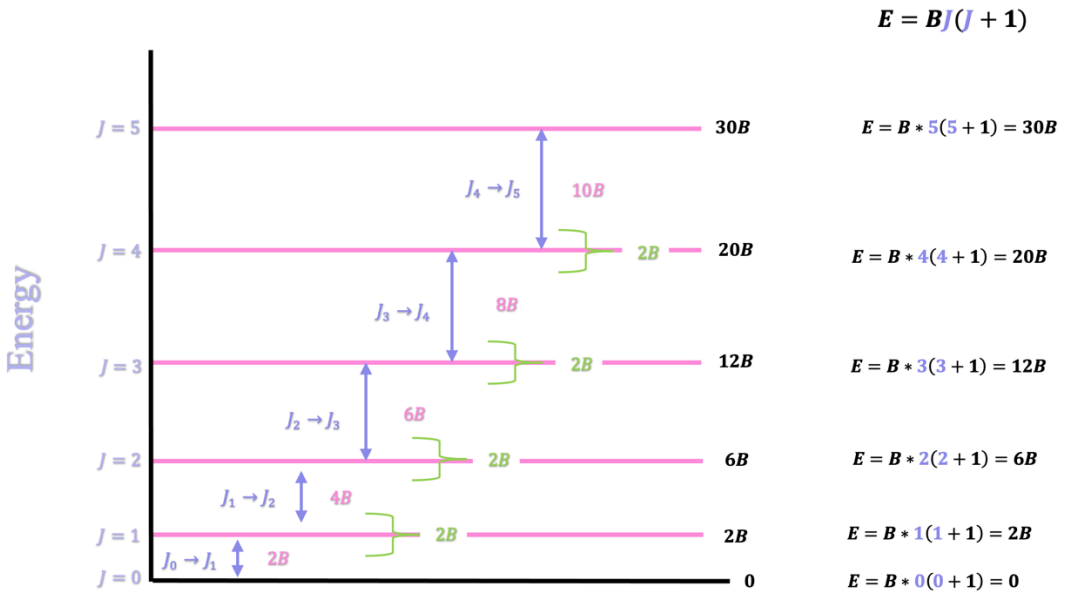

Figure 14: Selection rules for a Diatomic/Linear Molecule

If the allowed J values are plugged in ($J = 0,1,2,3 \ldots etc.$), it can be noted that there will be a spacing difference of multiples of 2B between the energy of the rotational transitions E_J and E_{J+1}. This can be shown in equations 3.13 where the difference in between energy levels is

$$\Delta E = E_{J+1} - E_J = \frac{h^2}{4\pi^2 I}(J+1) \tag{3.13}$$

Which can then be written in terms of the rotational constant B

$$\Delta E = 2B(J+1) \tag{3.14}$$

Where

$$B = \frac{h}{8\pi^2 I} \tag{3.15}$$

in the units of Hz. [63, 64, 87, 88, 97] As stated previously, the spacings of the rotational transitions differ by a 2B spacing. In a rotational spectrum, the spectral lines represent the rotational transitions of the energy diagram that are spaced by multiples of 2B. Therefore, in a rotational

spectrum, you will have evenly spaced lines by a factor of 2B when the molecule is being treated as a rigid body. An example of a rotational spectra for the diatomic or linear molecule, carbonyl sulfide, can be seen in Figure 15.

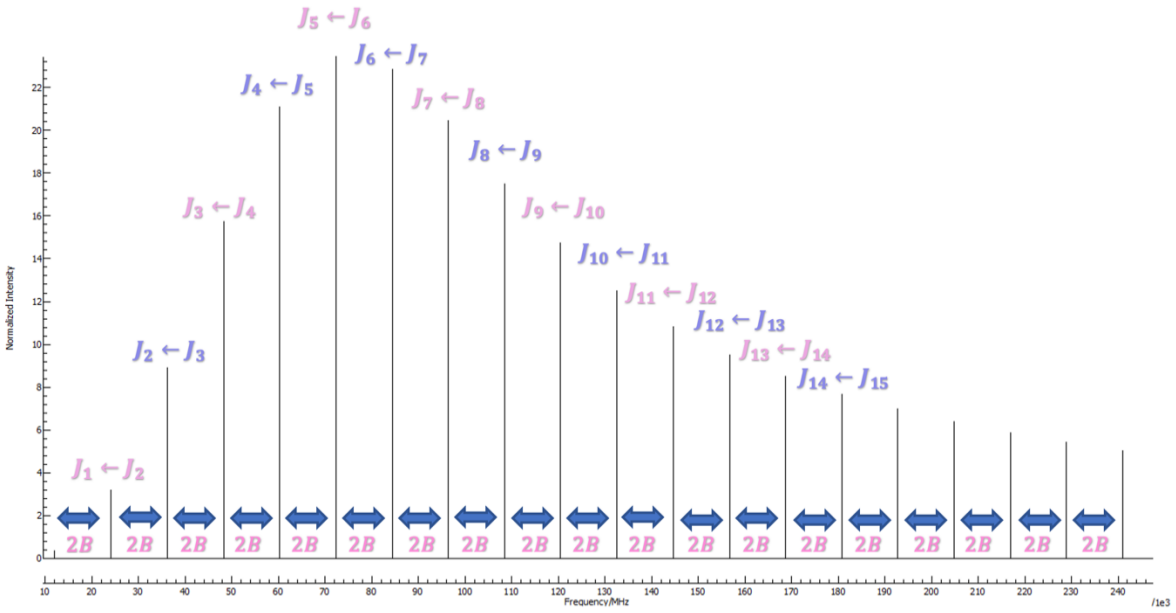

Figure 15: Rotational Spectra for carbonyl sulfide

The case for a diatomic/linear molecule previously discussed is the groundwork to talking about the molecule of focus for this thesis; fluorosulfonic acid. Fluorosulfonic acid is a molecule categorized in the asymmetric top with rotational constants A, B, and C being unequal to each other. In this case, A is greater than B which is greater than C meaning that the moment of inertia I_C will be the greatest and the spectrum will be physically different than for that of the linear/diatomic molecule. For an asymmetric top, the scenario is similar and can fall back on and can be seen as a linear combination of the symmetric top. In a symmetric top, two moments of inertia are the same and the remaining one is a non-zero value. In this scenario, there isn't only one angular momentum J describing the whole system. Now there is another angular momentum called K that represents the for the other 2 moments of inertia and describes the motion happening

regarding the principal axis of the molecule. For a symmetric top, there is also an external axis quantized in values of $M_J\hbar = 0, \pm 1, \ldots \pm J$ coming from possible external fields. The terms of rotation for a symmetric top follow that $\Delta J = \pm 1$, and $K = 0, \pm 1, \ldots \pm J$. When $K = -1$, also knowns as K_a, the molecule will follow a prolate symmetric top rotor. A good way to describe the physical description of a molecule is that it will look like a cigar placed vertically. When $K = +1$, also knowns as K_c, the molecule will follow the oblate symmetric top. This type of symmetric rotor will look extended and look like an egg flipped horizontally. When $K = 0$, the molecule will follow an asymmetric top which is the case for fluorosulfonic acid. Selection rules for a symmetric top include $\Delta \mathrm{J} = \pm 1, \Delta M_J = 0, \Delta \mathrm{K} = 0$.

When discussing the asymmetric top, all three moments of inertia are different. Actually, the solution to the Schrödinger's equation can be obtained by utilizing a symmetric top basis set. Ray's asymmetry parameter shown in equation 3.16 can best be used to describe the level of asymmetry in deviation from the prolate/oblate molecules. [18]

$$k = \frac{2B - A - C}{A - C} \tag{3.16}$$

The selection rules for an asymmetric top are more complex and are dependent on the 3 distinct dipole moments μ_a, μ_b, and μ_c. The rules consist of that $\Delta \mathrm{J} = 0, \pm 1$, and $\Delta M_J = 0, \pm 1$. However, there are different scenarios that happen for K_a and K_c. An a-type transition follows that $\mu_a \neq 0$ and $\mu_b = \mu_c = 0$, $K_a = 0, (\pm 2, \pm 4 \ldots)$ and $K_c = \pm 1, (\pm 3, \pm 5 \ldots)$. The purpose of K_a and K_c values are that the values inside the parenthesis are least likely to happen due to them being weaker. In a b-type transition, $\mu_b \neq 0$ and $K_a = K_c = \pm 1, (\pm 3, \pm 5 \ldots)$. For a c-type transition, $\mu_c \neq 0$ and $K_a = \pm 1, (\pm 3, \pm 5 \ldots)$ and $K_c = 0, (\pm 2, \pm 4 \ldots)$. The cases of the selection rules can be seen in Figure 16.

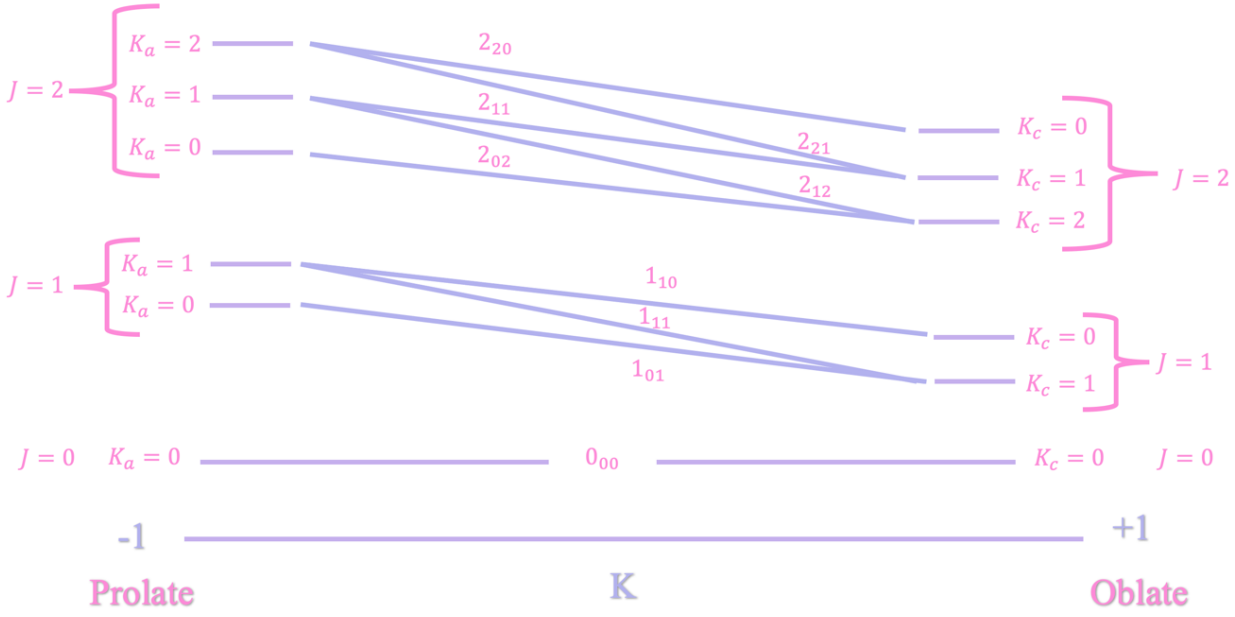

Figure 16: Selection rules for an asymmetric top

3.3 Centrifugal Distortion Constant

The centrifugal distortion constant, also known as the parameter D_J, is necessary to talk about in this thesis because we need to take into consideration the stretching motion of the molecule that it happens to have when in the middle of natural rotation. When a molecule rotates, it is not stiff as theoretically explained in the rigid rotor. A molecule rotating in a 3-D space will naturally have the bond stretching as it rotates. Figure 17 shows a picture describing that stretching motion of the molecule as it is rotating. This can be related to a mass on a spring and the equation from physics Hooke's law or the harmonic oscillator to study the vibrational behavior of the molecule in between the atoms.

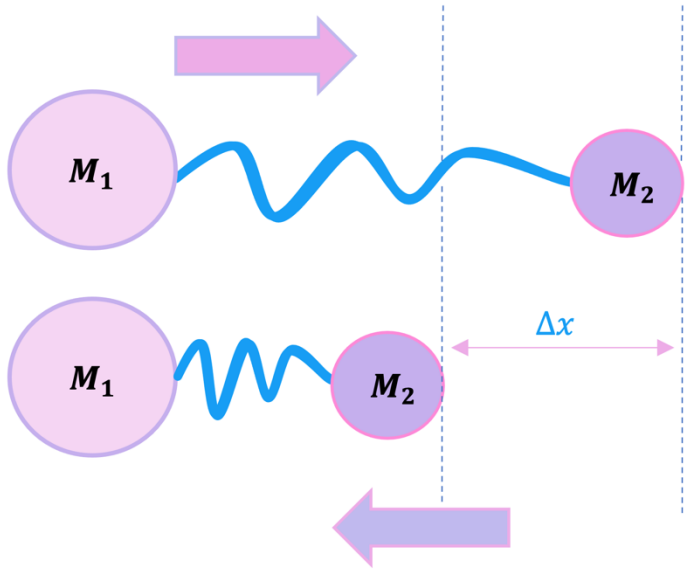

Figure 17: Stretching motion describing the centrifugal distortion constant

In the Schrödinger's equation, the Hamiltonian taking into account for the centrifugal distortion constant is shown in equation 3.17.

$$\widehat{H}_{CD} = -D_J \hat{J}^4 \tag{3.17}$$

This is a correction that is added to the original Hamiltonian of the rigid rotor where the constant D_J is

$$D_{J=} \frac{4B_e^3}{\omega_e^2} \tag{3.18}$$

In this equation, B_e stands for the rotational constant and $\omega_e$stands for the connection to the vibrational frequency. [35] Equation 3.19 shows resulting energy from a rigid rotor alone after the centrifugal distortion correction has been added from the case of a rigid rotor.

$$E_J = BJ(J+1) - D_J(J(J+1))^2 = \Big(B - D_J J(J+1)\Big) J(J+1) \tag{3.19}$$

When talking about the transition spacings in the spectrum in a more concrete matter, the expression for the correction of the centrifugal distortion constant is as shown in equation 3.20.

$$E_{J+1} - E_J = B[(J+1)(J+2) - J(J+1)] - D[(J+1)^2(J+2)^2 - J^2(J+1)^2]$$

$$= 2B(J+1) - 4D(J+1)^3 \tag{3.20}$$

As the molecule rotates faster, and the J values increase, the centrifugal distortion correction can become from negligeable to having a considerable effect on the spectrum. This correction of the centrifugal distortion constant will make the spectral lines be closer together due the increment in bond length and moment of inertia that will ultimately result in a lower rotational constant value. [3, 76] Figure 18 shows the effect of the centrifugal distortion constant that happens to the rotational spectrum from a rigid to a non-rigid body.

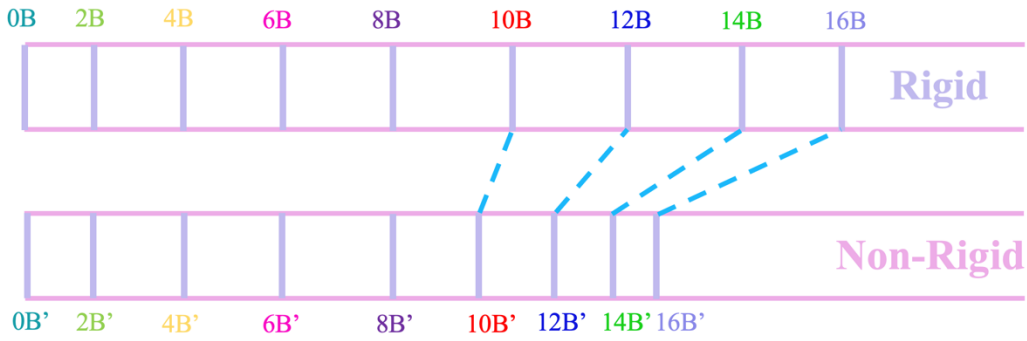

Figure 18: Effects of the centrifugal distortion constant to the rotational spectrum

For symmetric tops, the Hamiltonian for centrifugal distortion constant expands further and is composed of 2 more parameters, D_{JK} and D_K besides the original D_J. The expression can be seen in equation 3.21.

$$\hat{H}_{CD} = -D_J\hat{J}^4 - D_{JK}\hat{J}^2\hat{J}_z^2 - D_k\hat{J}_z^4 \tag{3.21}$$

The energy for the symmetric top is further divided based on which type of symmetric top we are discussing. For example, the prolate symmetric top will have a resulting energy shown by equation 3.22.

$$E_{J,K} = BJ(J+1) + (A-B)K^2 - D_J J^2(J+1)^2 - D_{JK}J(J+1)K^2 - D_K K^4 \tag{3.22}$$

For an oblate symmetric non-rigid rotor, the equation for the energy would be

$$E_{J,K} = 2B(J+1) - 4D_J(J+1)^3 - 4D_{JK}(J+1)K^2 \tag{3.23}$$

For an asymmetric top, there will be other 2 parameters that must be considered in order to describe well the spectra. These parameters come from Watson's A-reduced form of distortable rotor and include δ_J, and δ_K besides the already known D_J, D_{JK}, and D_K. [78] The Energy for the non-rigid rotor of an asymmetric top can be seen as follows:

$$E_{J,K} = -D_J J^4 - D_{JK} J^2 J_z^2 - D_k J_z^4 - \delta_J J^2 - \delta_K J_Z^2 \tag{3.24}$$

CHAPTER IV

COMPUTATIONAL WORK

4.1 Introduction

When discussing computational work in the field of chemistry, we use computers to process all the calculations needed to solve for the Schrödinger's equation and get information about the molecule. A Hamiltonian from the Schrödinger's equation for a molecular system in involves a kinetic and potential energy portion as shown in equation 4.1.

$$\widehat{\mathrm{H}} = \mathrm{T} + \mathrm{V} \tag{4.1}$$

The kinetic energy, symbolized by T, is composed of a summation involving all the particles in a molecule and can be represented by equation 4.2. [68]

$$\mathrm{T} = \frac{-\hbar^2}{2}\sum_i \frac{1}{m_i}\left(\frac{\partial^2}{\partial x_i^2} + \frac{\partial^2}{\partial y_i^2} + \frac{\partial^2}{\partial z_i^2}\right) = \frac{-\hbar^2}{2}\sum_i \frac{1}{m_i}\nabla_i^2 \tag{4.2}$$

The potential energy, symbolized by V, can be explained with the help of equation 4.3.

$$\mathrm{V} = \frac{1}{4\pi\varepsilon_0}\sum_j \sum_{k\neq j} \frac{e_j e_k}{\Delta r_{jk}} \tag{4.3}$$

In this equation, the Δr_{jk} represents the distance between particles j and k and the e_j and e_k represent the charge of the particle of interest. [23] Furthermore, the Hamiltonian for a molecular system while taking into consideration the kinetic and potential energy together with the particle interactions can be seen in equation 4.4. In this equation, we are taking into account

the electron-nuclear attraction, the electron-electron repulsion, and the nuclear-nuclear repulsion.

$$\widehat{H} = \frac{-\hbar^2}{2}\sum_{A}^{Nuclei}\frac{1}{m_A}\nabla_A^2 - \frac{\hbar^2}{2}\sum_{i}^{Electrons}\frac{1}{m_i}\nabla_i^2 - \frac{1}{4\pi\varepsilon_0}\sum_{A,i}^{Nuc.-Ele.}\frac{e^2 Z_A}{\Delta r_{Ai}} + \frac{1}{4\pi\varepsilon_0}\sum_{i\neq k}^{Electrons}\frac{e^2}{\Delta r_{ik}} + \frac{1}{4\pi\varepsilon_0}\sum_{A\neq B}^{Nuclei}\frac{e^2 Z_A Z_B}{\Delta r_{AB}} \quad (4.4)$$

The first 2 terms in equation 4.4 describe the kinetic energy from the nuclei and the electrons while the next 4 terms take into consideration of the potential energy. Term 3 describes the nuclear-electron attraction, and terms 4 and 5 take into account for the repulsive potential energy forces in between the electrons themselves and the nuclei themselves. [31, 45, 93] From this equation, we can eliminate a few terms revolving around the nucleus due to the Born-Oppenheimer's approximation that helps simplify the solution to the Schrödinger's equation. The Born-Oppenheimer's approximation states that we can treat the nucleus as if it were stationary because the nucleus is way heavier and slower than the electrons. [82] This allows for the Hamiltonian to be written in terms of a model that is dependent parametrically on the nucleus and its coordinates. [86]. The Hamiltonian equation describing a model following the Born-Oppenheimer's approximation is as follows:

$$\widehat{H} = -\frac{\hbar^2}{2}\sum_{i}^{Electrons}\frac{1}{m_i}\nabla_i^2 - \frac{1}{4\pi\varepsilon_0}\sum_{A,i}^{Nuc.-Ele.}\frac{e^2 Z_A}{\Delta r_{Ai}} + \frac{1}{4\pi\varepsilon_0}\sum_{i\neq k}^{Electrons}\frac{e^2}{\Delta r_{ik}} \quad (4.5)$$

The kinetic and potential energy involving the nuclei can be removed, leaving the equation with three terms that involve the electrons.

In the mid-1950's, chemists started using the use of computers to obtain quantitative results of molecular behavior through the solution of the Schrödinger's equation. [15] The work behind this thesis involves the use of quantum chemical calculations through the use of a program called

Gaussian 16. In this program, we used Ab initio calculations which encompassed the use of several methods and a selected basis set.

Methods in computational chemistry are different approaches used to help calculate a computational solution to the Schrödinger's equation. A method that was used in the project of this thesis was the *Ab initio* method. *Ab initio* methods focus on approximate solutions to the energies of the Schrödinger's equation solely based on the quantum mechanical laws and theory involving well-known physics' constants and not experimental data. *Ab initio* methods will help calculate for the electron density, electronic energy, rotational constants, dipole moments and other properties. [24, 109] This method uses high amounts of numerical computations and the more complex the molecule, the longer time the calculations take. [69] Within this branch of the *Ab initio* method, there are several methods that were used to calculate a solution to the Schrödinger's equation. In an orderly fashion, the methods used in this thesis were the Hartree-Fock (HF), the Density Functional Theory (B3LYP), and the second order Møller-Plesset perturbation Theory (MP2).

Within the Ab *initio* method of calculations, a basis set was also used to help ease the calculations in regards to solving the Schrödinger's equation. Basis sets are linear combinations of a set of functions that describe the physical location of space of molecular orbitals. [75] The basis that was utilized for the work of this thesis is the aug-cc-pVTZ or the Augmented Correlation Consistent Polarized Split-Valence Triple Zeta basis set created by Dunning and coworkers. In this basis set, the "aug" stands for augmented and it means that there is an extra diffuse basis function added to each atom and angular momentum such that the basis set is augmented fully. As an example, for fluorosulfonic acid, you will have the addition of diffuse s, p, d, and f subshells on the Carbon atom. [70] This will help accurately represent the atomic orbitals that are most far

away from the nucleus. [68] The "-cc-" stands for correlation consistent and is a type of extended basis set that adds up shells of functions to the atomic functions of Hartree-Fock. [73] The "p" stands for polarized and considers the inclusion of polarization functions that contain an additional node and allowing the orbitals to be more asymmetric about the atomic nucleus. This will create the ending effect of expanding the basis set and obtaining more accurate calculations by allowing additional flexibility in the basis set. [68] The "VTZ" ending stands for split-valence triple zeta and utilizes 3 slater type orbitals (STOs) to represent a single atomic orbital. It includes the split-valence and two orbitals linearly combined of the same type but different effective charges. This helps in expanding the flexibility to generate adjustable sizes of atomic orbitals. [22, 25] In a short summary, this is a huge basis set introduces the possibility of having various different atomic orbitals that can be chosen the make the molecular orbitals.

4.2 Hartree-Fock Theory

The Hartree-Fock (HF) method was a collaboration between D.R. Hartree and V. Fock to help obtain better approximations for the wavefunction and the energies of a multi-electron chemical system. For most cases, the Hartree-Fock method is known as a good starting point and the first step for higher accuracy approximations in solving the electronic Schrödinger's equation that arises from the time-independent Schrödinger's equation after the Born-Oppenheimer approximation model is applied. [80] Hartree-Fock focuses in taking into consideration the potential repulsive energy interaction from the electron of interest and the distributed average field generated by the rest of the electrons in the system. [31] This method involves treating the electronic wavefunction as a one-electron wavefunction combined into a single slater determinant as shown by equation 4.6.

$$\psi(r) = \frac{1}{\sqrt{n!}}\left(\begin{vmatrix} \phi_1(r_1)\alpha(1) & \phi_1(r_1)\beta(1)\ldots & \phi_{\frac{n}{2}}(r_1)\alpha/\beta(1) \\ \phi_1(r_2)\alpha(2) & \phi_1(r_2)\beta(2)\ldots & \phi_{\frac{n}{2}}(r_2)\alpha/\beta(2) \\ \phi_1(r_n)\alpha(n) & \phi_1(r_n)\beta(n) & \phi_{\frac{n}{2}}(r_n)\alpha/\beta(n) \end{vmatrix}\right) \quad (4.6)$$

The resulting best possible one-electron wavefunction will yield to the lowest energy for a multi-electron system. [31] Therefore, the multi-electron problem system is solved by considering it a one-electron problem where each specified spin electron will contain its own orbital. This will result in twice the number of orbitals accounting for the electrons and their corresponding spin. The symbols ϕ represent the orthonormal set of molecular orbitals from a range of 1 to $\frac{n}{2}$ to account for the totality of the spatial orbitals. The variable n represents each electron with its specified spin that is being alternated as the label of the electron spin, n, ranges from 1 to n. In this case, spin up is represented by α and spin down is represented by β. [19, 23, 91] The slater determinant representing the antisymmetric electronic wavefunction is then used to derive the Fock operator from the Hartree-Fock equation. The Hartree-Fock equation can be seen in equation 4.7.

$$\hat{\mathrm{F}}\varphi_i = \epsilon_i\varphi_i \quad (4.7)$$

In this equation, $\hat{\mathrm{F}}$ is the Fock operator that focuses on giving the energy and the HF orbital for a single electron. The derived Fock operator can be best described by equation 4.8.

$$\hat{\mathrm{F}} = KE + PE(nucleus - Electron) + \sum_{j=1}^{N}\left(2\hat{J}_j - \hat{K}_j\right) \quad (4.8)$$

The first two terms in equation 4.7 represent the kinetic energy of the electrons and the potential energy regarding the attractive forces between the electrons and the nucleus. The third term is the potential energy of the single electron interaction from the rest average field of electrons. The $\hat{J}$ operator is the Coulomb operator that deals with the electron repulsive interactions and $\hat{K}$ is the exchange operator relating to the change of orbital labels. After the electronic wavefunction is

applied as part of the Hamiltonian the energy can be calculated. With the help of the variational method, the expected energy can be worked out to be lower even though it is greater than the actual ground energy. [19, 31, 80] The energy of the Hartree-Fock can start by making an initial guess of the parameters of the spin orbitals from the Fock operator in the Hartree-Fock equation and solving for new sets of spin orbitals until it reaches self-consistency. The spin orbitals which yield the lowest electronic energy are the correct spin orbitals that are used to shape the lowest energy state of a molecule. [80, 91]

4.3 Density Functional Theory

The Density Functional Theory (DFT) method is similar to that of the Hartree-Fock but is a step higher up the ladder in terms of a more accurate approximation of the electron-electron interactions. As seen in equation 4.9, the electronic energy is distributed into several terms.

$$E = E_T + E_V + E_J + E_X + E_C \tag{4.9}$$

Similar to the Hartree-Fock Method, the first 3 terms represent the same energies. The E_T is the kinetic energy from the electron motion, E_V is the potential energy arising from the nuclear-electron attraction, and E_J is the potential energy from the electron-electron repulsion. The remaining two terms, E_X and E_C, are a correction to the electron-electron interaction that is treated in an average way from the HF method. The term E_X represents the electron exchange energy and the term E_C represents the electron correlation energy. Larger E_X values correct for the strong electronic repulsive forces for electrons with the same spin. The smaller E_C term accounts for the weaker repulsive force of electrons with opposite spin. [4] The term for the exchange functionals can be described as follows

$$E^X = \left(-\frac{3}{2}\left(\frac{3}{4\pi}\right)^{1/3} \int \rho^{4/3}\, d^3r\right) - \gamma \frac{\rho^{4/3}\left(\rho^{-4/3}|\nabla\rho|\right)^2}{\left(1+6\gamma \sin^{-1}\left(\rho^{-4/3}|\nabla\rho|\right)\right)} d^3 \tag{4.10}$$

Where γ is 0.0042 Hartrees from a parameter chosen to fit the exchange energies, $\rho(r)$ is the electron density and $\nabla\rho$ would refer to the gradients. The correlation functional can be described further with equation 4.11.

$$E^C = \int \rho\varepsilon_C(r_s(\rho(r)), \xi)d^3r \tag{4.11}$$

Where the variables r_s is the density parameter, ε_C is the equivalent to an expression involving the interpolation of mixed spin, and ξ is the spin polarization corresponding to α and β spins. The type of Density Functional Theory method that was used in this thesis is the B3LYP or the Becker 3-parameter, Lee, Yang, and Parr exchange correlation functional. This Density Functional is a hybrid functional of the exact Hartree-Fock exchange and the exchange-correlation terms in DFT. Equation 4.12 shows the hybrid density functional, B3LYP.

$$E_{XC}^{B3LYP} = (1 - a_0)E_x^{LSDA} + a_0E_x^{HF} + a_x\Delta E_x^{B88} + a_cE_c^{LYP} + (1 - a_c)E_c^{VWN} \tag{4.12}$$

In this equation, the terms E_x^{LSDA} and E_c^{VWN} come from the approximation of the spin density in the exchange and correlation functional from the density functional, the E_x^{HF} term comes from the exchange in the Hartree-Fock, the ΔE_x^{B88} is the correction of the gradient to the exchange functional and the E_c^{LYP} is the term for the Perdew-Wang gradient correction to the correlation functional. For this method, Backer placed the coefficients to be $a_0 = 0.2$, $a_x = 0.72$, and $a_c = 0.81$. [20, 85]

4.4 Second Order MØller-Plesset Perturbation Theory

The Møller-Plesset perturbation theory is another method of the *Ab initio* calculations that is very popular and relatively inexpensive. The Møller-Plesset perturbation theory follows the Rayleigh-Schrödinger perturbation theory and adds a perturbation of higher excitations to the HF field-approximation to further improve on the energy results. [23, 28] This method uses

mathematical techniques of the many-body perturbation theory. In this case, the Hamiltonian is divided into:

$$\hat{H} = \hat{H}_0 + \lambda\hat{V} \tag{4.13}$$

The correction added to the Hamiltonian will consist of $\lambda\hat{V}$ where λ is a dimensionless parameter and $\hat{V}$ is a small perturbation that can be expressed in terms of a power series to the perturbed wavefunction and energy. [106] The way this correction is added can be seen in equations 4.14 and 4.15.

$$\psi = \psi^{(0)} + \lambda\psi^{(1)} + \lambda^2\psi^{(2)} + \lambda^3\psi^{(3)} + \cdots \tag{4.14}$$

$$E = E^{(0)} + \lambda E^{(1)} + \lambda^2 E^{(2)} + \lambda^3 E^{(3)} + \cdots \tag{4.15}$$

These set of equations can therefore be plugged back to the Schrödinger's equation as shown by equation 4.16.

$$(\hat{H}_0 + \lambda\hat{V})(\psi^{(0)} + \lambda\psi^{(1)} + \lambda^2\psi^{(2)} + \cdots) = (E^{(0)} + \lambda E^{(1)} + \lambda^2 E^{(2)}+\ldots)\,(\psi_0 + \lambda\psi^{(1)} + \lambda^2\psi^{(2)} + \cdots) \tag{4.16}$$

After factoring in the variables and setting them by terms of λ, one can get to the conclusion that the set of equations representing the energies from $E^{(0)}$ to $E^{(2)}$ are described by the following equations 4.17 through 4.19.

$$E^{(0)} = \langle\psi^{(0)}|\hat{H}_0|\psi^{(0)}\rangle = \sum_i \varepsilon_i \tag{4.17}$$

$$E^{(1)} = \langle\psi^{(0)}|\hat{V}|\psi^{(0)}\rangle \tag{4.18}$$

$$E^{(2)} = \langle\psi^{(0)}|\hat{V}|\psi^{(1)}\rangle = -\sum_t \frac{|\langle\psi^{(0)}|\hat{V}|\psi_t\rangle|^2}{E_t - E^{(o)}} \tag{4.19}$$

The zeroth order perturbation is equivalent to the sum of the orbital energies. The sum of the $E^{(0)}$ and $E^{(1)}$ will give the Hartree-Fock energy since that energy is represented by $\hat{H}_0 + \hat{V}$. Once $\psi^{(1)}$is

solved for then the $E^{(2)}$ can be calculated which results in a negative correction to lower the energy of the initial Hartree-Fock energy. [23, 96] Equation 4.20 then goes on to show that the energy for a second perturbation can be written in tems of the spin-orbitals. [28]

$$E_0^{(2)} = -\frac{1}{4}\sum_{ab}^{Virt}\sum_{ij}^{Occ}\frac{|\langle ab||ij\rangle|^2}{\varepsilon_a+\varepsilon_b-\varepsilon_i-\varepsilon_j} \tag{4.20}$$

Where the equation is in terms of the virtual terms, a and b, and the occupied terms, i and j, that are responsible for the electron coupling.

4.5 Coupled-Cluster Theory

Coupled-cluster theory with single and double excitations (CCSD) applies an exponential factor of n excitations to the cluster operator, $\hat{T}$, that takes into account for the slater determinants as shown by equation 4.21. [33, 116]

$$\Psi_{CC} = e^{\hat{T}_n}\Psi_{HF} \tag{4.21}$$

In which the cluster operator will stop at the second excitation for the single and double excitations of but can have as many excitations as the number of electrons in the system.

$$\hat{T} = \hat{T}_1 + \hat{T}_2 + \hat{T}_3 + \cdots \hat{T}_n \tag{4.22}$$

For the double excitation cluster operator, $\hat{T}_2$, it takes into account the amplitudes expansion coefficients, t, and the first and second excitations as shown in equation 4.23.

$$\hat{T}_2\Psi_{HF} = \sum_{i<j}^{occ}\sum_{a<b}^{virt} t_{ij}^{ab}\,\Psi_{ij}^{ab} \tag{4.23}$$

The exponential form of the cluster operator with up to the second excitation is written in the form of a power series expansion as shown by equation 4.24 [33]

$$e^{\hat{T}_2} = \sum_{k=0}^{\infty}\frac{\hat{T}_2^k}{k!} = 1 + \hat{T}_2 + \frac{\hat{T}_2^2}{2!} + \frac{\hat{T}_2^3}{3!} + \cdots \tag{4.24}$$

When the coupled cluster wavefunction is plugged back into the Schrödinger's equation, the equation turns into equation 4.25.

$$e^{-\hat{T}_2}\hat{H}e^{\hat{T}_2}\Psi_{HF} = E_{CC}\Psi_{HF} \tag{4.25}$$

In this equation, the complex conjugate of the exponential operator, $e^{-\hat{T}_2}$ is needed to generate deexcitations to help generate the reference wavefunction. [40] Once the Schrödinger's equation is solved for, the solution can yield to the energy of a molecular system that was obtained through the use of the coupled cluster single double excitation theory method. For the work of this thesis, the Coupled Cluster with Single, Double excitations, and a perturbed Triple excitation (CCSD(T)) was used. In this case, we would want to resemble to the Coupled Cluster with Single, Double, and Triple excitations (CCSDT) and achieve approximate treatments to that of adding a triple excitation of slater determinant, $\hat{T}_3$, where

$$\hat{T} = \hat{T}_1 + \hat{T}_2 + \hat{T}_3 \tag{4.26}$$

However, we would add that triple excitations through perturbation theory. The scaling used for CCSD(T) in comparison to CCSDT would be the ϑM^7 instead of ϑM^8. Where the size of the system size is decreased by only a power. This would still contain a very good execution time. The energy for a CCSD(T) can be obtained by adding the corrections of the perturbation expansion of the triple amplitudes to that of the CCSD energy as shown by equation 4.27.

$$E_{CCSD(T)} = E_{CCSD} + \frac{1}{36}\sum_{ijk}^{abc} t_{ijk}^{abc*} D_{ijk}^{abc} t_{ijk}^{abc} + \frac{1}{4}\sum_{ijk}^{abc}\langle jk\|bc\rangle t_i^{a*} t_{ijk}^{abc} \tag{4.27}$$

The first term in the equation would symbolize the energy of the CCSD level, the second and term would symbolize the correlation of the third- and fourth- order perturbation theory. In which the D_{ijk}^{abc} involves the elements from the Fock matrix that are in the diagonal positions. [66, 116]

CHAPTER V

ROTATIONAL STUDIES OF FLUOROSULFONIC ACID AND ITS HYDRATES

5.1 Previous works

This chapter will focus on the work done throughout the two years of master's degree on flourosulfonic acid which is the first derivative of perfluorooctanesulfonic acid. In addition, fluorosulfonic acid is a superacid widely used in organic synthesis, electrochemical technologies, and petrochemical applications. This chapter will start with previous work done on this molecule by other research groups and move on to the updated continuation of the studies for this molecule. In 2005, the theoretical work on the dissociation of fluorosulfonic acid with water in microsolvated clusters was published. The methods used for this work include the Density Functional Theory (B3LYP) and the second-order Møller-Plesset Perturbation Theory (MP2) with the 6-311++G** basis set. In this work, the clusters for flourosulfonic acid HSO_3F-$(H_2O)_n$ ranged with $n = 1 - 3$.Results for this work shows that it takes a total of 3 water molecules to break off fluorosulfonic acid and leaving it with its conjugate base SO_3F^-. [50] In 2006, another paper was published in which they studied different halosulfonic acids with the inclusion of fluorosulfonic acid using DFT and MP2 methods with a 6-311++G basis set. In this work, fluorosulfonic acid was looked at with water clusters HSO_3F-$(H_2O)_n$ ranging with $n = 1 - 4$. More information was obtained from the different types of conformers regarding the di- and tri-hydrate water molecule. The results of this work were also in agreement with that of the first where it takes up to 3 water molecules to

dissociate fluorosulfonic acid and leaving behind its conjugate base. [49] The current work on fluorosulfonic acid also supports that conclusion.

5.2 Monomer results of theoretical work

The theoretical work for fluorosulfonic acid includes that of the HF, DFT, MP2, and some of the work in CCSD(T) ab initio calculation methods with the aug-cc-pVTZ basis set. For the monomer of fluorosulfonic acid, there was a starting potential energy scan that was generated to take into account for the different types of possible low-energy conformers. The scan was done along the dihedral angle $\tau(H_6\text{-}O_2\text{-}S_1\text{-}F_5)$ for every 10° and 36 steps of rotation for a total of a 360° angle. Figure 19 shows the potential energy scan with the results of 2 low-energy conformers of equivalent structures shown at the bottom wells.

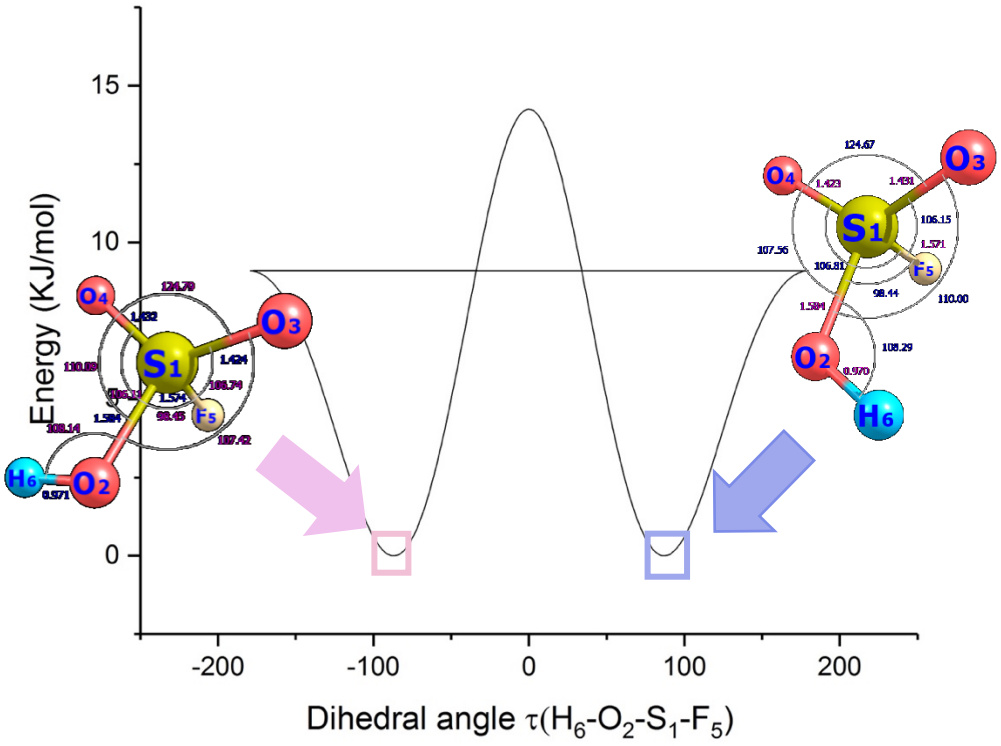

Figure 19: Potential Energy Surface Scan for Fluorosulfonic acid monomer along the dihedral angle $\tau(H_6\text{-}O_2\text{-}S_1\text{-}F_5)$

From this starting work, there was a geometry optimization for each equivalent conformer. Table 6 describes all the parameters that came out from the optimization geometry for the monomer that apply to both conformers. The rotational constants (A, B, C), dipole moments (μ_a, μ_b, μ_c) bond lengths (r) and bond angles ($\angle$) are reported.

Table 6: Fluorosulfonic acid monomer theoretical results

Parameter	B3LYP	MP2	CCSD(T)
A (MHz)	4927.3	4962.2	4973.8
B (MHz)	4883.9	4941.1	4944.3
C (MHz)	4814.7	4852.6	4864.4
μ_a(Debye)	1.3	2.0	-
μ_b(Debye)	1.9	0.55	-
μ_c (Debye)	1.7	1.9	-
r(O_2H_6)	0.970	0.971	0.971
r(S_1O_2)	1.593	1.583	1.584
r(S_1O_3)	1.424	1.424	1.424
r(S_1O_4)	1.432	1.432	1.432
$\angle$ ($S_1O_2H_6$)	109.31	108.15	108.14
$\angle$ ($O_2S_1O_3$)	107.54	107.43	107.42
$\angle$ ($O_2S_1O_4$)	110.14	110.06	110.09
$\angle$ ($O_3S_1O_4$)	124.54	124.78	124.79
$\angle$ ($F_5S_1O_2$)	98.48	98.44	98.45
$\angle$ ($F_5S_1O_3$)	106.77	106.75	106.74
$\angle$ ($F_5S_1O_4$)	106.18	106.14	106.11

Figure 20 shows the detailed structure for the equivalent structures of the monomer. The two equivalent energy structures can be thought of resulting from the flipping motion of the OH group or the tunneling motion of the proton. Proton tunneling would be described as the quantum jump of a proton that disappears its original location and appears in an adjacent position to which is separated by a potential energy barrier. [83] The proton is very light and can potentially instantaneously pass through the barrier and switch locations from one side of the oxygen 2

aligning with the oxygen 4 to the other side of oxygen 2 aligning with the oxygen 3. A similar effect in the hydrogen behavior is seen in the hydrate complexes that lead to different conformers.

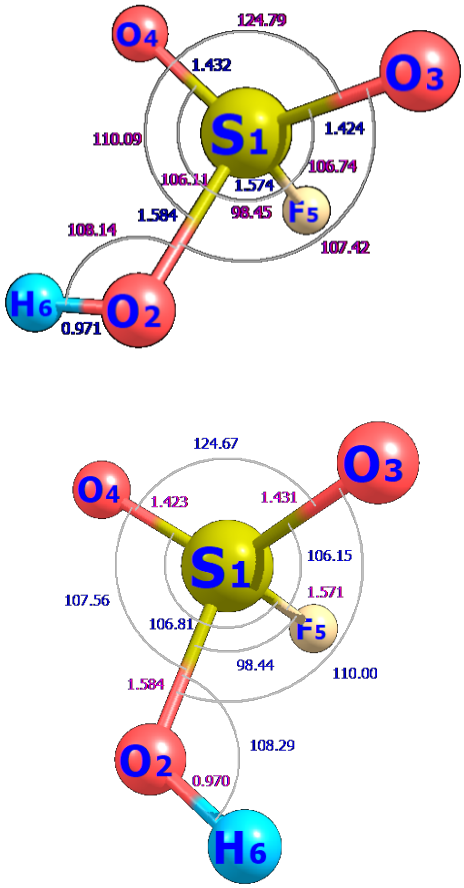

Figure 20: Structure for the two equivalent structures of conformer 1

Figure 21 show the simulated rotational spectra for fluorosulfonic acid monomer. As seen by the information in the table 6, based on the MP2 results of the dipole moments, the monomer will have mostly a- and c-type transitions.

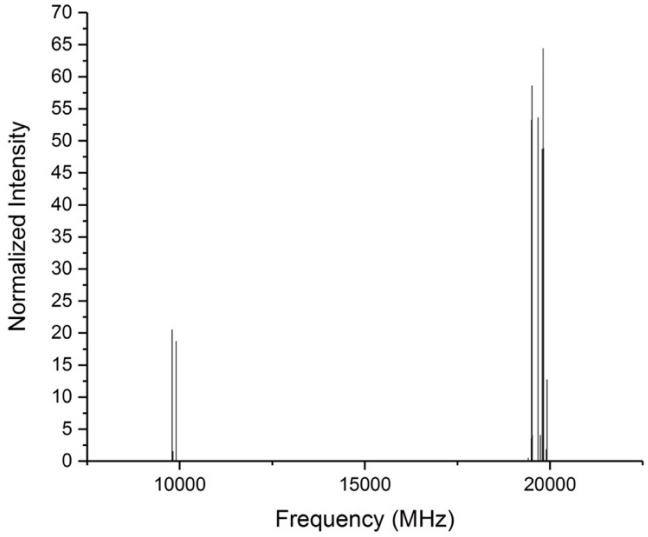

Figure 21: Rotational Spectrum for conformer 1 of fluorosulfonic acid monomer

5.3 Monohydrate results of theoretical work

The monohydrate theoretical results for fluorosulfonic acid can be seen in Table 7 and Figures 22-23. In Table 7, it is shown that there were two convergences for two conformers. As seen by the table, the two conformers they are very close in energy. With the correction added of the Zero-point energy, they end up switching places as to which one is the lowest conformer. The rotational constants and dipole moments were reported in the DFT and MP2 methods for both conformers. From the information provided by table 7, the resulting accurate structures and the rotational spectra were simulated. Figures 22 and 23 show in detail the resulting structure of both conformers as fluorosulfonic acid comes in contact with one water molecule. It can be seen that in Figures 22 and 23 shows there is a plane between atoms O_2, H_6, H_8 and O_4 with the presence of a free hydrogen represented by H_9. The lowest energy conformer, represented by Figure 22, shows the free hydrogen pointing upwards towards the orientation of the fluorine atom while conformer 2 has the free hydrogen pointing the opposite direction. Figures 24 shows the simulated rotational

spectra for conformer 1 where we would be able to observe the a-type and b-type transitions. Figure 25 shows the simulated spectrum for conformer 2 where a-type transitions are the most prominent and the b-type transitions are hardly observed. Since both are similar in rotational constants, figures 26 and 27 were generated to be able to see the a-type and b-type transitions individually and for comparison purposes.

Table 7: Theoretical results for fluorosulfonic acid monohydrate

Monohydrate				
	Conformer 1		**Conformer 2**	
Parameters	**B3LYP**	**MP2**	**B3LYP**	**MP2**
ΔD (KJ/mol)	**0.008**	**0.004**	**0**	**0**
ΔD_0 (KJ/mol)	**0**	**0**	**0.055**	**0.036**
A (MHz)	**4869.5**	**4918.5**	**4884.8**	**4938.3**
B (MHz)	**1862.3**	**1915.2**	**1859.9**	**1911.3**
C (MHz)	**1847.3**	**1901.3**	**1845.9**	**1898.6**
μ_a(Debye)	**4.3**	**4.1**	**4.6**	**4.4**
μ_b(Debye)	**1.8**	**1.9**	**0.46**	**0.47**
μ_c (Debye)	**0.21**	**0.41**	**0.18**	**0.20**
r(O_2H_6)	**1.007**	**1.007**	**1.008**	**1.008**
r(S_1O_2)	**1.563**	**1.555**	**1.564**	**1.556**
r(S_1O_3)	**1.426**	**1.425**	**1.426**	**1.425**
r(S_1O_4)	**1.441**	**1.441**	**1.441**	**1.441**
∠ ($S_1O_2H_6$)	**109.31**	**107.99**	**109.30**	**108.01**
∠ ($O_2S_1O_3$)	**109.67**	**109.57**	**109.69**	**109.58**

∠ ($O_2S_1O_4$)	110.51	110.52	110.39	110.38
∠ ($O_3S_1O_4$)	122.93	123.06	122.81	122.94
∠ ($F_5S_1O_2$)	99.32	99.32	99.42	99.42
∠ ($F_5S_1O_3$)	106.31	106.4	106.33	106.43
∠ ($F_5S_1O_4$)	105.25	105.1	105.43	105.29

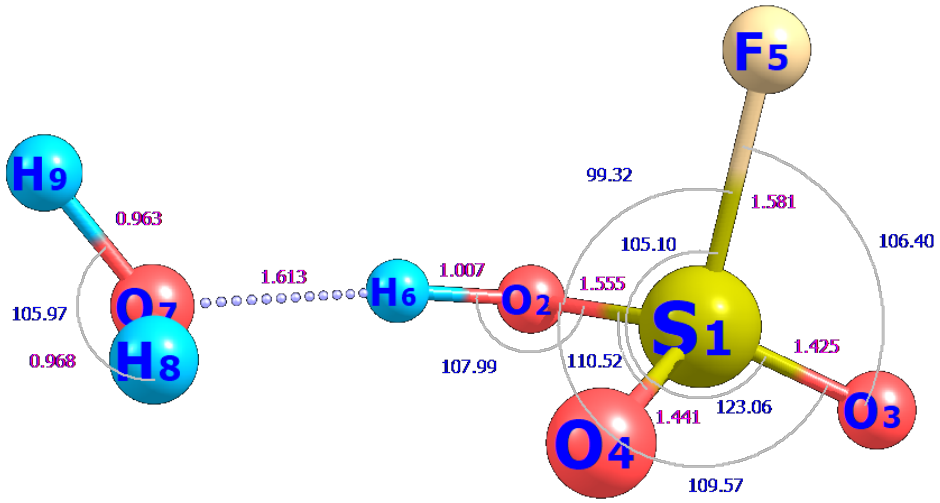

Figure 22: Structure for fluorosulfonic acid monohydrate first conformer

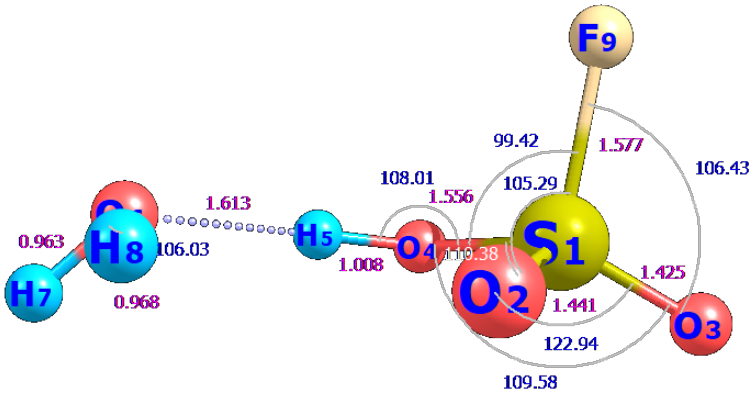

Figure 23: Structure for fluorosulfonic acid monohydrate second conformer

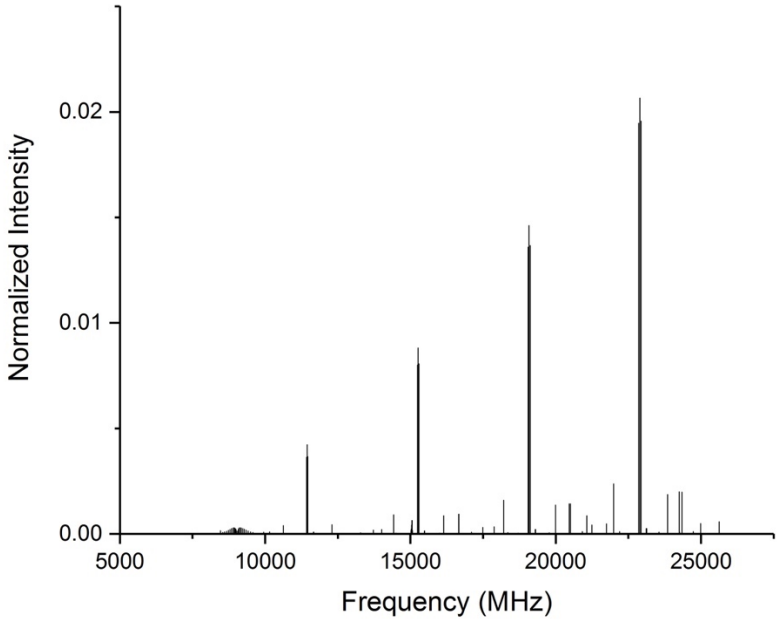

Figure 24: Rotational spectrum for the first conformer of the monohydrate

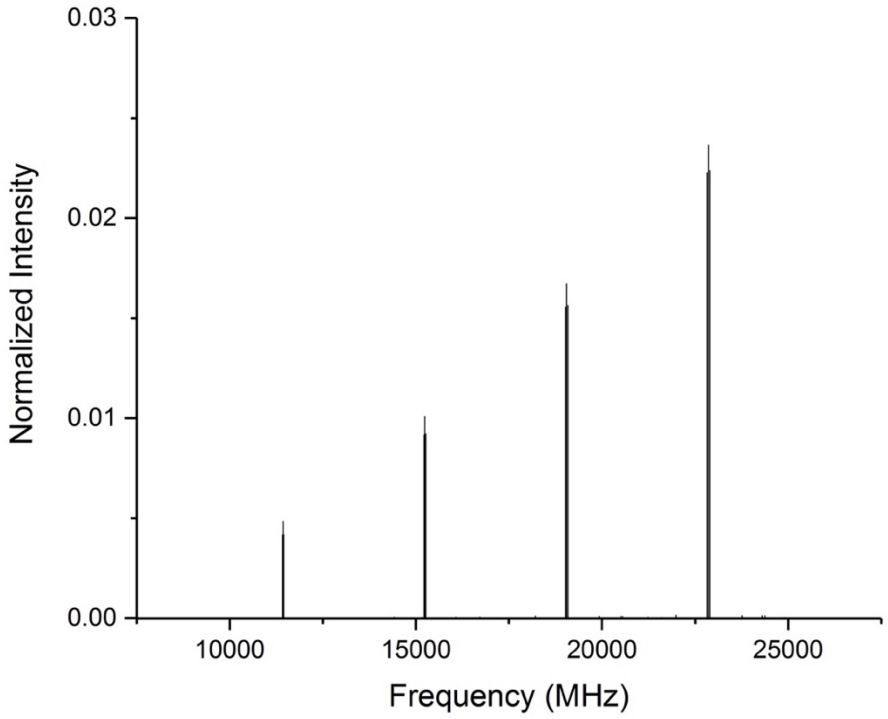

Figure 25: Rotational spectrum for the second conformer of the monohydrate

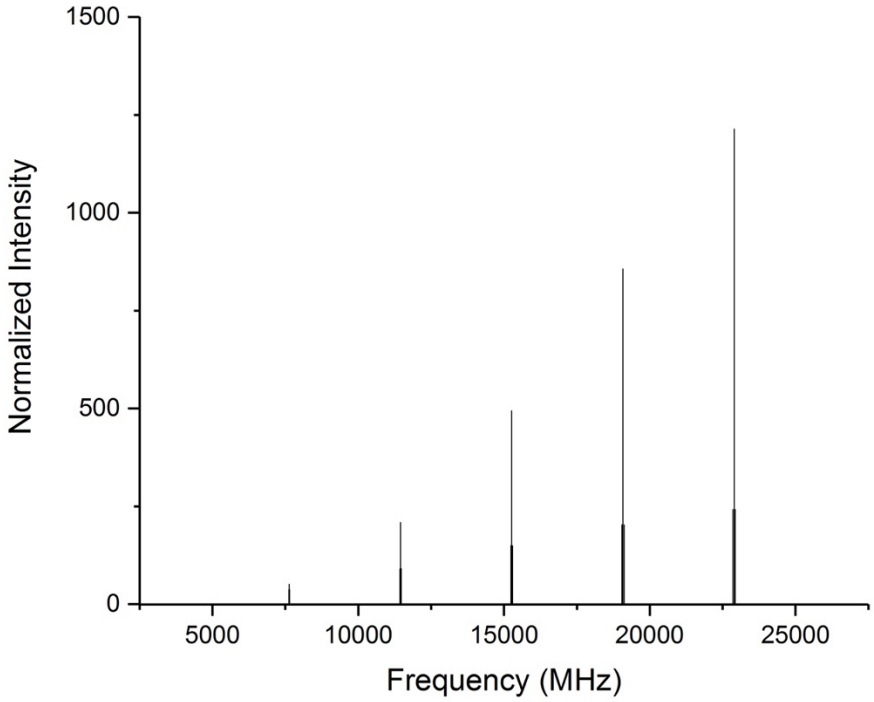

Figure 26: Monohydrate spectrum with only a-type transitions

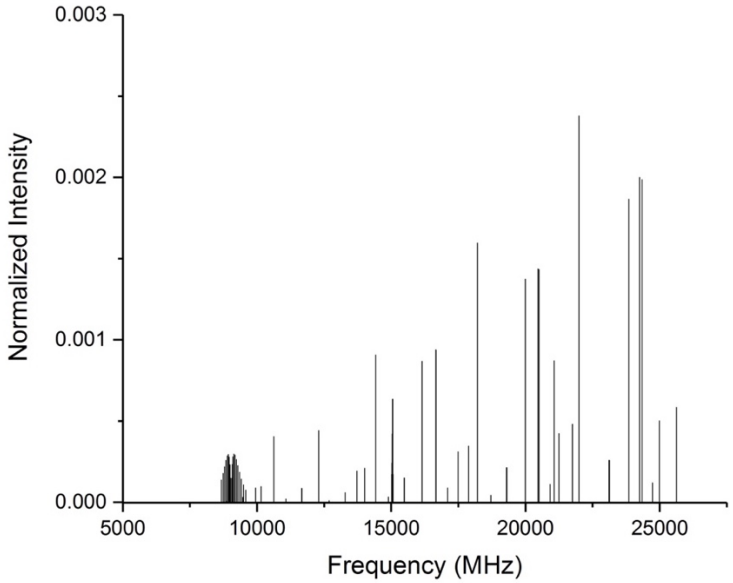

Figure 27: Monohydrate spectrum with only b-type transitions

5.4 Dihydrate results of theoretical work

The dihydrate theoretical results for fluorosulfonic acid can be seen in table 8 and figures 28-36. In this case, there was the convergence of five conformers. The rotational values and dipole moments were reported in the DFT and MP2 methods for all the conformers with the exception of conformer 5. Figure 28-32 show the resulting accurate structure for fluorosulfonic acid dihydrate with its bond lengths and bond angles. Conformer 1 being the lowest energy is very close in energy with conformer 2. After conformer 2, the deviation is greater when moving on to conformers 3, 4 and 5. In between conformers 3 and 4, there is also a small difference in energy. Conformer 5 reveals to be the conformer with the highest energy as to the data of the DFT file. For this conformer, the MP2 calculation was not able to converge. Structurally speaking, similar to the case of the monohydrate, there is a plane formed by the atoms O_2, O_4, H_{12}, H_8, O_7, and H_6 with the addition of two free hydrogens H_9 and H_{11}. Conformer 1 has the positions of the H_9 facing down and the H_{11} facing up. Conformer 2, which is close in energy, shows the free hydrogens flipped in the opposite direction. Conformer 3 contains both of the free hydrogen facing the upwards direction and conformer 4 has them facing the downward direction. Conformer 5 shows a completely different conformer in which there is a bridge in between the H_6 and the F_5 by water molecules instead of the H_6 to one of the Oxygen atoms available. Figures 33-34 show the simulated rotational spectrum for the first two conformers of the dihydrate of flourosulfonic acid. In these spectra, only a-type transitions are prominent.

Table 8: Theoretical results for fluorosulfonic acid dihydrate

Dihydrate										
	Conformer 1		Conformer 2 (du)		Conformer 3 (uu)		Conformer 4 (dd)		Conformer 5	
Parameters	B3LYP	MP2	B3LYP	MP2	B3LYP	MP2	B3LYP	MP2	B3LYP	MP2
ΔD (KJ/mol)	0	0	0.368	0.464	2.317	2.284	2.574	2.738	12.8	-
ΔD_0 (KJ/mol)	0	0	0.314	0.410	1.765	1.758	2.049	2.18	11.4	-
A (MHz)	3015.1	3054.8	3009.9	3038.8	2999.0	3037.7	3006.4	3041.3	2969.3	-
B (MHz)	1201.8	1226.2	1203.4	1242.9	1205.4	1231.6	1194.1	1220.9	1249.3	-
C (MHz)	1051.5	1071.5	1050.8	1080.4	1052.2	1073.3	1042.3	1063.1	1071.6	-
μ_a(Debye)	4.4	4.3	4.5	4.3	4.3	4.1	4.8	4.7	4.8	-
μ_b(Debye)	0.46	0.45	0.41	0.30	0.38	0.37	0.58	0.54	0.61	-
μ_c (Debye)	0.58	0.61	0.60	0.58	2.7	2.7	1.5	1.5	0.35	-
r(O_2H_6)	1.044	1.038	1.039	1.038	1.037	1.036	1.037	1.035	1.034	-
r(S_1O_2)	1.543	1.539	1.545	1.538	1.545	1.539	1.546	1.539	1.550	-
r(S_1O_3)	1.595	1.426	1.426	1.426	1.426	1.426	1.427	1.426	1.427	-
r(S_1O_4)	1.445	1.444	1.445	1.444	1.445	1.443	1.445	1.444	1.436	-
∠ ($S_1O_2H_6$)	113.5	111.79	113.94	112.08	113.67	111.73	113.87	112.03	111.46	-
∠ ($O_2S_1O_3$)	110.14	109.94	110.04	109.99	109.99	109.92	109.94	109.89	109.73	-
∠ ($O_2S_1O_4$)	111.83	111.71	111.80	111.64	111.94	111.77	111.72	111.52	111.99	-
∠ ($O_3S_1O_4$)	121.2	121.58	121.32	121.59	121.41	121.64	121.30	121.57	123.13	-
∠ ($F_5S_1O_2$)	99.94	99.9	100.00	99.92	99.90	99.82	100.06	100.00	98.99	-
∠ ($F_5S_1O_3$)	106.72	106.71	106.56	106.67	106.57	106.68	106.60	106.69	105.59	-
∠ ($F_5S_1O_4$)	104.49	104.43	104.58	104.45	104.46	104.38	104.73	104.64	104.16	-

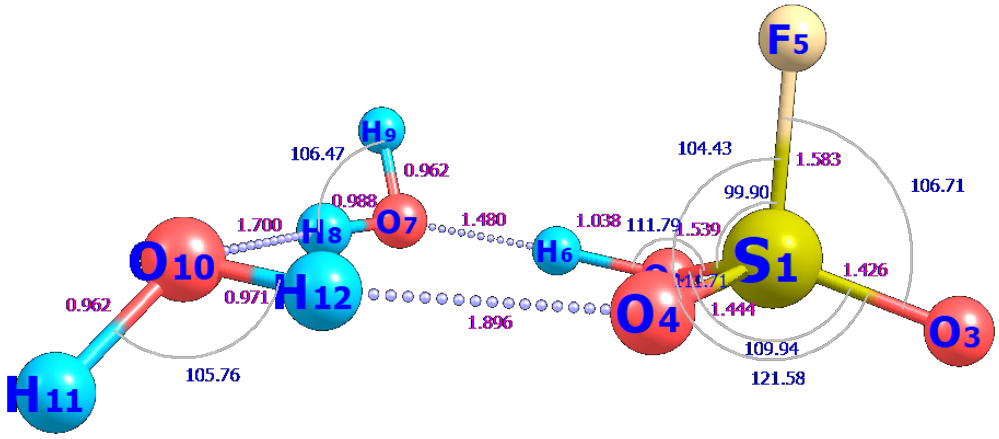

Figure 28: Structure for fluorosulfonic acid dihydrate first conformer

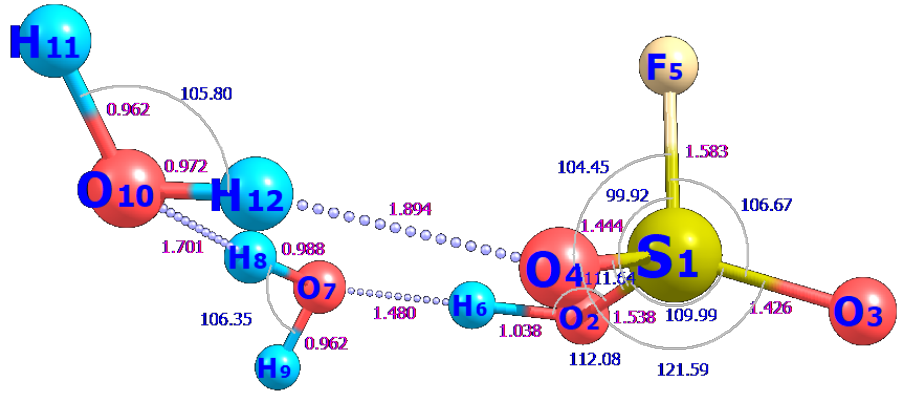

Figure 29: Structure for fluorosulfonic acid dihydrate second conformer

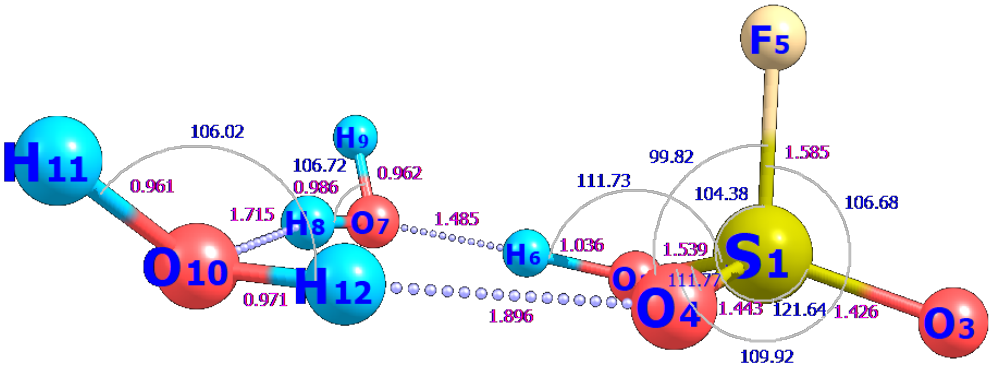

Figure 30: Structure for fluorosulfonic acid dihydrate third conformer

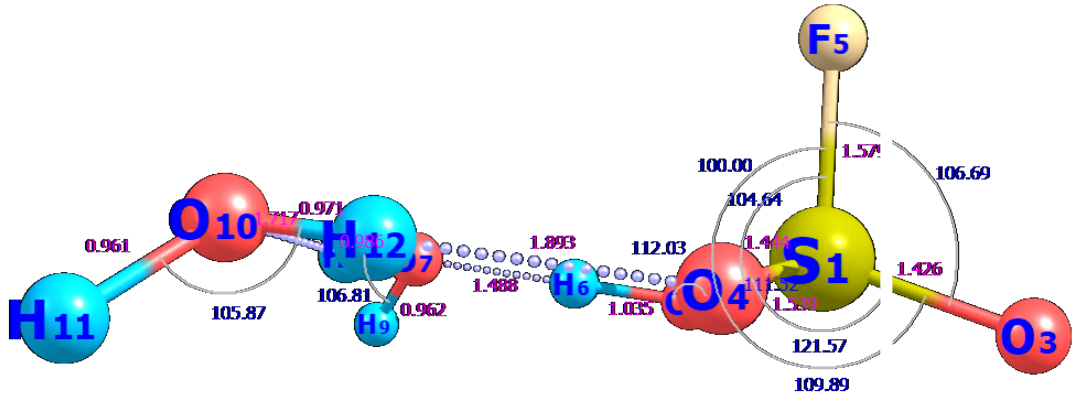

Figure 31 Structure for fluorosulfonic acid dihydrate fourth conformer

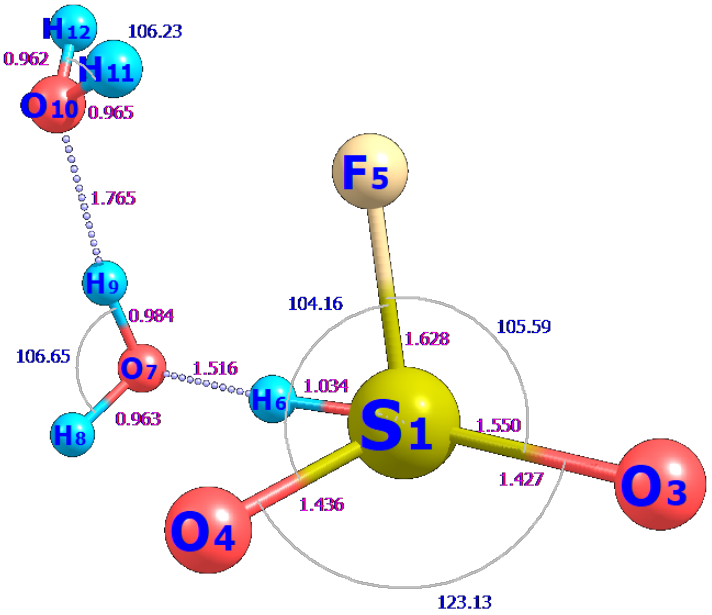

Figure 32: Structure for fluorosulfonic acid dihydrate fifth conformer

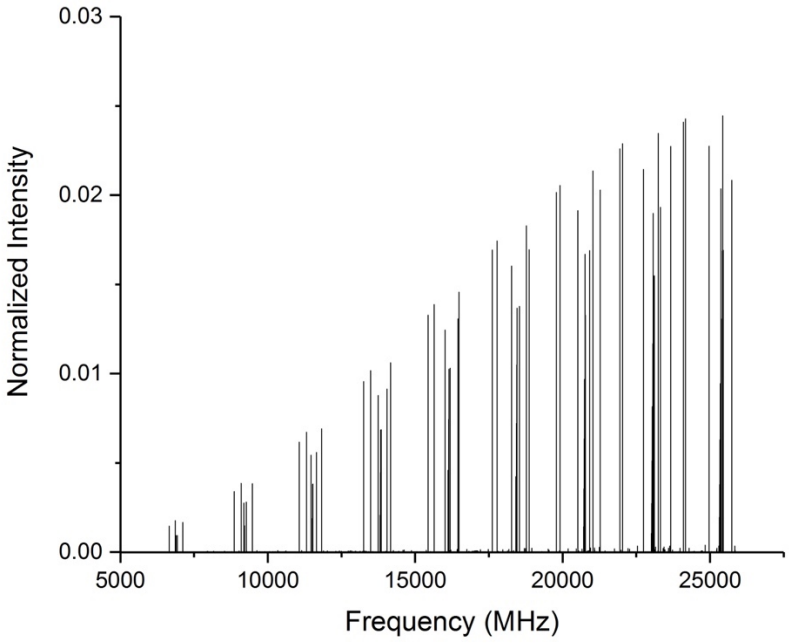

Figure 33: Rotational Spectrum for fluorosulfonic acid dihydrate first conformer

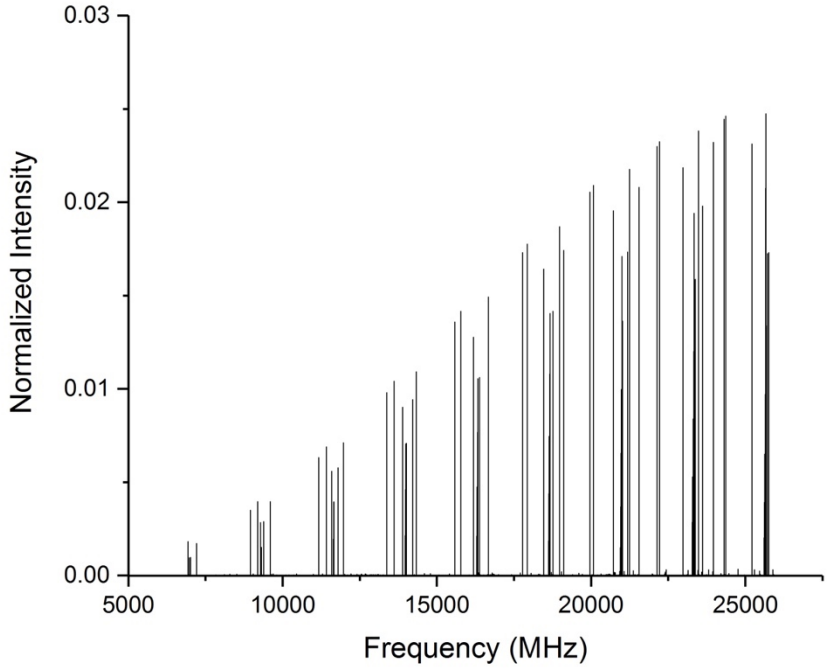

Figure 34: Rotational spectrum for fluorosulfonic acid dihydrate second conformer

5.5 Trihydrate results of theoretical work

The trihydrate theoretical data can be seen in table 9 and figures 35-38. As seen from table 9, there was a convergence for a total of 3 conformers and therefore the respective energies for each conformer were included. The rotational values and dipole moments for each conformer and each method was also reported. From the theoretical results in Table 9, it can be seen that conformer 1 was the lowest energy conformer and therefore the most stable one. Conformers 2 and 3 have about 8 and 10 KJ/mol of higher energy. Figure 35 represents the accurate structure of conformer 1, the lowest energy conformer, with its bond lengths and bond angles. Similarly, Figures 36 and 37 show the accurate structures for conformers 2 and 3 with their bond lengths and angles. Finally, figure 38 show the simulated rotational spectra for the first conformer of fluorosulfonic acid trihydrate. As indicated by table 9, the a-type transitions will be seen the

strongest. There will also be some of c-type that will be noticeable and none of the b-type transitions.

Table 9: Theoretical results for fluorosulfonic acid trihydrate

Trihydrate						
	Conformer 1		Conformer 2		Conformer 3	
Parameter	B3LYP	MP2	B3LYP	MP2	B3LYP	MP2
ΔD (KJ/mol)	0	0	8.0	11.5	6.7	15.3
ΔD_0 (KJ/mol)	0	0	5.7	8.9	2.0	10.3
A (MHz)	1786.23	1808.35	1729.17	1755.51	1868.56	1862.18
B (MHz)	1102.33	1117.72	1081.27	1097.68	845.91	927.04
C (MHz)	863.5	877.93	842.26	858.47	672.09	726.18
μ_a(Debye)	4.5	4.3	5.8	5.6	4.6	4.4
μ_b(Debye)	0.0	0.0	0.59	0.93	0.48	0.23
μ_c (Debye)	1.0	1.1	0.43	0.43	0.77	0.93
$r(O_2H_6)$	1.532	1.517	1.441	1.421	1.053	1.056
$r(S_1O_2)$	1.482	1.479	1.487	1.485	1.538	1.531
$r(S_1O_3)$	1.46	1.458	1.433	1.432	1.427	1.427
$r(S_1O_4)$	1.46	1.458	1.461	1.459	1.446	1.447
$\angle (S_1O_2H_6)$	111.71	110.89	116.9	115.11	115.15	112.48
$\angle (O_2S_1O_3)$	113.8	113.89	115.37	115.33	110.28	110.43
$\angle (O_2S_1O_4)$	113.8	113.89	113.4	115.83	111.79	111.48
$\angle (O_3S_1O_4)$	115.71	115.7	118.4	118.65	121.08	121.43
$\angle (F_5S_1O_2)$	102.68	102.57	100.32	100.44	100.2	100.15
$\angle (F_5S_1O_3)$	104.46	104.41	104.2	104.21	106.54	106.58

∠ ($F_5S_1O_4$)	104.46	104.41	101.65	101.46	104.48	104.2

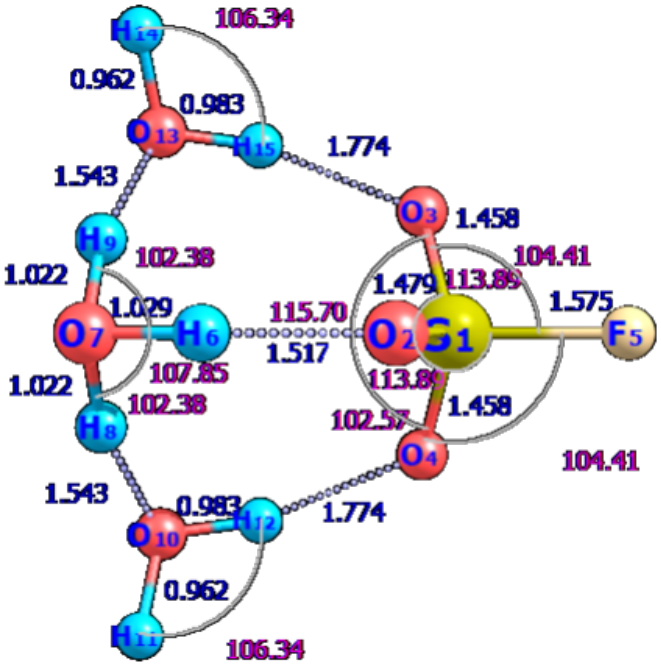

Figure 35: Structure for conformer 1 of fluorosulfonic acid trihydrate

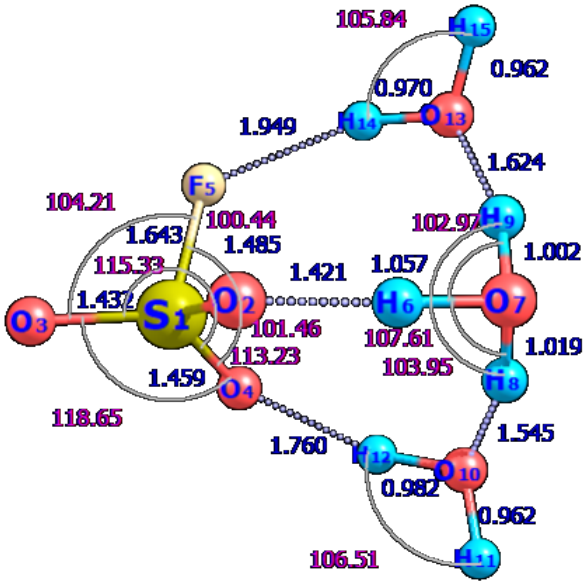

Figure 36: Structure for conformer 2 of fluorosulfonic acid trihydrate

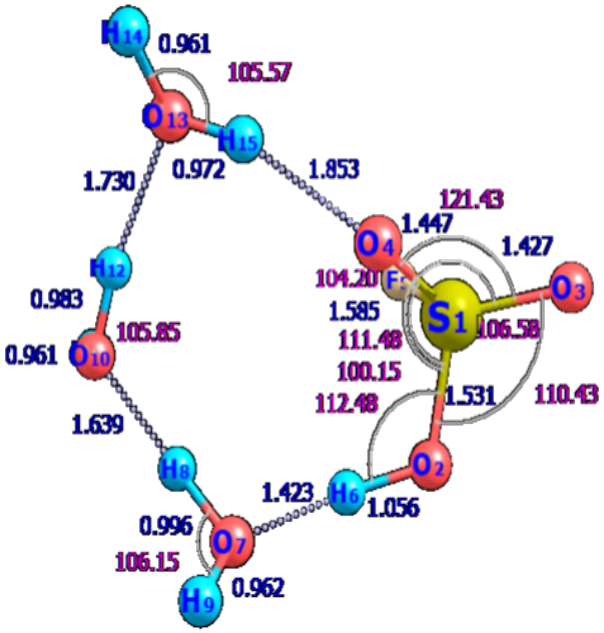

Figure 37: Structure for conformer 3 of fluorosulfonic acid trihydrate

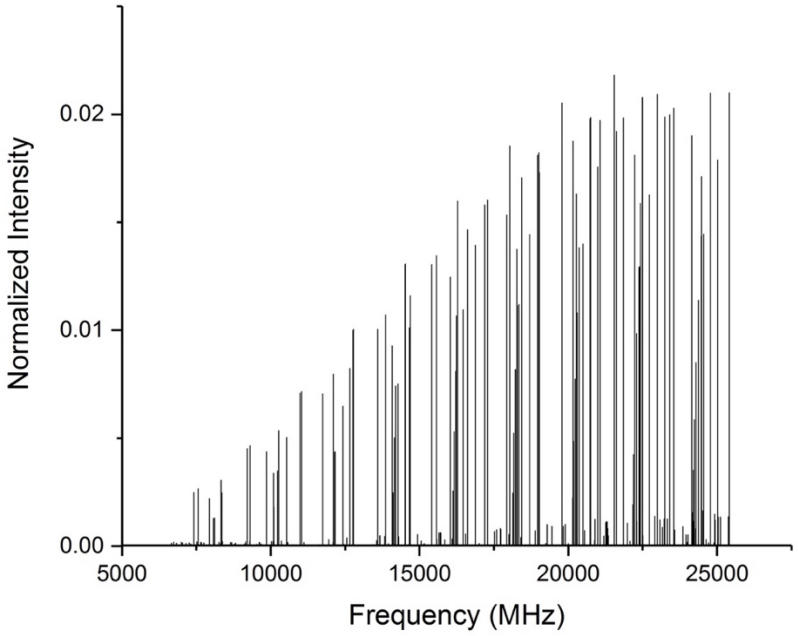

Figure 38: Rotational spectrum for conformer 1 of fluorosulfonic acid trihydrate

To finalize the theoretical results, Figure 39 shows how the fluorosulfonic acid would dissociate or detach as it interacts with the water. The numerical order shows the progression on the behavior of fluorosulfonic as it interacts with the addition of one water molecule at the time. Number 1 would show the monomer of fluorosulfonic acid, number 2 the monohydrate, number 3 the dihydrate and number 4 the trihydrate. The full dissociation can be observed in number 4 where the fluorosulfonic acid is broken up by 3 water molecules.

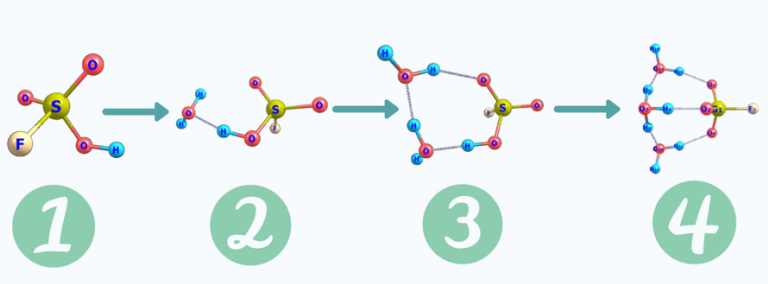

Figure 39: Dissociation of fluorosulfonic acid

CHAPTER VI

CONCLUSION

The environmental contaminant, PFOS, has been bioaccumulating into the environment since the 1950's. Due to the bioaccumulation throughout the years, PFOS has gotten into the soil, air, snow, and water. Therefore, bioaccumulation of PFOS has also been found in the animals and human blood. There have been several reports in between the potential bioaccumulation and several health complications in animals and humans. Therefore, it is crucial to prevent further bioaccumulation of this toxic contaminant. This research focused on the detailed studies of the derivatives of PFOS, starting with fluorosulfonic acid. In addition, there was also a focus on an environmental work done in Putian, China for the importance of creating a baseline documentation of the amount of perfluorinated contaminants and other environmental contaminants in the southern part of China. It is important to be aware and keep track of this contaminant that has been found worldwide. Within this work, we aim to increase the knowledge on the technical and detailed information that makes up this molecule to be able to stop the bioaccumulation and be able to remove it from our environment.

REFERENCES

[1] Arrieta-Cortes, R, Fabrias, P, Hoyo-Vadillo, C, Kleiche-Dray, M, 2017. Carcinogenic risk of emerging persistent organic pollutant perfluorooctane sulfonate (PFOS): A proposal of classification. Reg. Tox. and Pharm., 83, 66-80.

[2] Atkins, P., De Paula, J., & Keeler, J. (2017). Atkins' physical chemistry (11th ed.). Oxford University Press.

[3] Banwell, C.N. (1983). Fundamentals of Molecular Spectroscopy Third Edition. 56-58. [4] Baseden, K., Tye*, J. W. (2014). Introduction to Density Functional Theory: Calculations by Hand on the Helium Atom. *J. Chem. Educ.* 2014, 91, 12, 2116–2123. https://doi.org/10.1021/ed5004788

[5] Bernath, P. (2020). Spectra of Atoms and Molecules (4th ed.). Oxford University Press.

[6] Bosanac, D. S. (2001). Rigid rotor in phase space. 9-10. Retrieved from https://arxiv.org/pdf/quant-ph/0104094.pdf.

[7] Business & Human Rights Resource Centre. (n.d.). Retrieved September 18, 2020, from https://www.business-humanrights.org/en/latest-news/dupont-lawsuits-re-pfoa-pollution-in-usa/

[8] Butt, C, Berger, U, Bossi, R, Tomy, G, 2010. Levels and trends of poly- and perfluorinated compounds in the arctic environment. Science of the Total Environment, 408, 2936-2965.

[9] Cahoon, L. B. (2019). Chapter 13 - GenX Contamination of the Cape Fear River, North Carolina: Analytical Environmental Chemistry Uncovers Multiple System Failures. *Separation Science and Technology*, 11, 341-354.

[10] Carrillo, M. (2020). The Rotational Spectrum of 1,1-Diiodoethane, Thesis. The University of Texas Rio Grande Valley.

[11] Castellan, G. W. (1983). Physical Chemistry (3rd Edition). 503-507

[12] Chen, C-Y., Chen, Y-T., Chen, K-S., Hsu, C-=C., Liu, L-L., Chen, H-S., Chen, M-H. (2018). Arsenic and five metal concentrations in the muscle tissue of bigeye tuna

(Thunnus obesus) in the Atlantic and Indian Oceans. *Marine Pollution Bulletin*, 129, 186-193.

[13] Chong, Z, Wei, Y, Zhifeng, Y, 2010. Environmental flows management strategies based on the spatial distribution of water quality, a case study of Baiyangdian Lake, a shallow freshwater lake in China. *Procedia Environ. Sci*., 896-905.

[14] Christou, M, Fraser, T, Berg V, Ropstad, E, Kamstra, J, 2020. Calcium signalling as a possible mechanism behind increased locomotor response in zebrafish larvae exposed to a human relevant persistent organic pollutant mixture of PFOS. Environmental Research, 187, 109702.

[15] Committee on Mathematical Challenges from Computational Chemistry, National Research Council. (1995). Mathematical Challenges from Theoretical/Computational Chemistry. Ch. 2, 13.

[16] Conti, A, Stazzeri, C, Rhoden, K, 2019. Perfluorooctane sulfonic acid, a persistent organic pollutant, inhibits iodide accumulation by thyroid follicular cells in vitro. Molecular and Cellular Endocrinology, 515, 110922.

[17] Cook, R. (2003). Microwave molecular spectroscopy. Encyclopedia of Physical Science and Technology (Third Edition), 798-852.

[18] Cooke, S.A., Ohring, P. (2012). Decoding Pure Rotational Molecular Spectra for Asymmetric Molecules. Journal of Spectroscopy, vol. 2013. Article ID 698392, 10 pages. https://doi.org/10.1155/2013/698392

[19] Cramer, C. J. (2004). Essentials of Computational Chemistry: Theories and Models (2nd Edition). Ed. Wiley & Sons. 124-126.

[20] Daniel, C. (2021). 2.15-Density Functional Theories and Coordination Chemistry. Comprehensive Coordination Chemistry III (Third Ed.) 256-275.

[21] European Food Safety Authority; Perfluoroalkylated substances in food: occurrence and dietary exposure. EFSA Journal 2012; 10(6):2743. [55 pp.] doi: 10.2903/j.efsa.2012.2743. Available online: www.efsa.europa.eu/efsajournal

[22] Extended Basis Sets. (2020, March 18). Retrieved October 11, 2021, from https://chem.libretexts.org/@go/page/210881

[23] Foresman, J., Frisch, Æ.,(1996).Exploring Chemistry with Electronic Structue Methods Second Edition. Gaussian Inc.

[24] Friesner, R. (2005). Ab *initio* quatum chemistry: Methodology and applications. https://doi.org/10.1073/pnas.0408036102

[25] Gaussian Basis Sets. (2020, March 18). Retrieved October 11, 2021, from https://chem.libretexts.org/@go/page/210880

[26] GB 17378.4-2007. The Specification for Marine Monitoring: Part 4: Seawater Analysis. China Standards Press; Shenzhen, China: 2007.

[27] Gordy, W., Cook, R. L. (1970). Microwave Molecular Spectra. Interscience Publishers, Inc.

[28] Götz, A. W., Wölfle, T., Walker, R. C. (2010). Chapter 2- Quantum Chemistry on Graphics Processing Units. Annual Reports in Computational Chemistry, 6, 21-35.

[29] Guo, Q, He, Z, Liu, X, Liu, B, Zhang, Y, 2019. High-throughput non-targeted metabolomics study of the effects of perfluorooctane sulfonate (PFOS) on the metabolic characteristics of A. thaliana leaves. Science of the Total Environment, 710, 135542.

[30] Habibullah-Al-Mamun, M., Ahmed, M. K., Raknuzzaman, M., Islam, M. S., Negishi, J., Nakamichi, S., Sekine, M., Tokumura, M., Masunaga, S. (2016). Occurrence and distribution of perfluoroalkyl acids (PFAAs) in surface water and sediment of a tropical coastal area (Bay of Bengal coast, Bangladesh). *Science of The Total Environment*. 571, 1089-1104.

[31] Hanson, D. M., Harvey, E., Sweeney, R., & Zielinski, T. J. (2021, July 22). The Born-Oppenheimer Approximation. Retrieved October 9, 2021, from https://chem.libretexts.org/@go/page/1973

[32] Heart Disease Facts. (2020, September 08). Retrieved September 18, 2020, from https://www.cdc.gov/heartdisease/facts.htm

[33] Hofmann, M., Schaefer III, H.F. (2013). Computational Chemistry. Encyclopedia of Physical Science and Technolog (Third Edition), 487-506.

[34] Hogue, C. (2019). Governments endorse global PFOA ban, with some exemptions C&EN Global Enterprise 2019 97 (19), 5-5 DOI: 10.1021/cen-09719-leadcon

[35] Hollas, M. J. *Modern spectroscopy*. (4th ed.). Chichester: John Wiley & Sons, 2002, 111-112.

[36] Holzer, J., Lilienthal, H., Schuman, M. (2021). Human Biomonitoring (HBM)- I values for perfluorooctanoic acid (PFOA) and perfluorooctane sulfonic acid (PFOS) – Description, derivation and discussion. *Regulatory Toxicology and Pharmacology*. 121, 104862.

[37] Huang D-R., Wen Y-Y., Chen Z-H., Li R-L., Gong Z-B. (2016). Rapid analysis of perfluorinated compounds in coastal and estuarine seawater by SPE enrichment with

ultra-high-performance liquid chromatography-tandem mass spectrometry. FenXi CeShi XueBao(J. Instr. Anal.), 35, 305-310.

[38] HY/T 147.1-2013.Code of practice for marine monitoring technology Part 1: Seawater.

[39] Jacob, J. M., Karthik, C., Saratale, R. G., Kumar, S. S., Prabakar, D., Kadirvelu, K., Pugazhendhi, A. (2018). Biological approaches to tackle heavy metal pollution: A survey of literature. *Journal of Environment*, 217, 56-70.

[40] Jensen, F. (2007). Introduction to Computational Chemistry Second Edition. 169-171.

[41] Kuehl, D, Haebler, R, Potter, C, Lahvis, G, Donahue, M, Regal, R, 2009. PFOS and PFOSA in bottlenose dolphins: An investigation into two unusually high mortality epizootics. Reproductive Toxicology, 27, 421.

[42] Kuroda, K., Murakami, M., Oguma, K., Takada, H., Takizawa, S. (2014). Investigating sources and pathways of perfluoroalkyl acids (PFAAs) in aquifers in Tokyo using multiple tracers. *Science of The Total Environment*, 488-489, 51-60.

[43] Laboratory Testing. (n.d.). Retrieved September 18, 2020, from https://www.michigan.gov/pfasresponse/0,9038,7-365-86704_90691---,00.html

[44] Lerner, S. (2018, July 31). 3M Knew About the Dangers of PFOA and PFOS Decades Ago, Internal Documents Show. Retrieved September 18, 2020, from https://theintercept.com/2018/07/31/3m-pfas-minnesota-pfoa-pfos/

[45] Levine, I. (2009). Physical Chemistry (6th Edition). 676-682.

[46] Li, H, Wang, C, Huang, X, Hug, A, 2018. Spacial Assessment of Water Quality with Urbanization in 2007-2015, Shanghai, China.

[47] Li, L, Zheng, H, Wang, T, Cai, M, Wang, P, 2018. Perfluoroalkyl acids in surface seawater from the North Pacific to the Arctic Ocean: Contamination, distribution and transportation. Environ. Pollut., 238, 168-176.

[48] Li, R, Guo, C, Lin, X, Chan, T, Lai, K, Chen, J, 2020. Integrative omics analyses uncover the mechanism underlying the immunotoxicity of perfluorooctanesulfonate in human lymphocytes. Chemosphere, 256, 127062.

[49] Li, S., Tao,F., Gu. (2006). Theoretical study on the ionic dissociation of halosulfonic acids in small water clusters. Chemical Physics Letters, 426, 1-7.

[50] Li, S., Weber, K., Tao, F., Gu, R. (2005). Theoretical investigation of ionic dissociations of fluorosulfonic acid in microsolvated clusters. Chemical Physics, 232, 397-406.

[51] Li, T., Sun, G., Yang, C., Liang, K., Ma, S., Huang, L. (2018). Using self-organizing map for coastal water quality classification: Towards a better understanding of patterns and processes. *Science of The Total Environment*, 628-629, 1446-1459.

[52] Li, X-N., Al-Sabri, A., Ameen, F., Al-Dayan, N., Adnan, A., Yao, J. (2019). Genetic polymorphisms of 20 autosomal STR loci in the Han population of Putian City, Southeastern China. *Annals of Human Biology*, 46(6), 509-513.

[53] Lin, W. (1999). Fourier Transform Microwave Spectroscopy of Scandium Monohalides, Thesis. University of British Columbia.

[54] Liu, B., Wang, J., Xu, M., Zhao, L., Wang, Z. (2019). Spatial distribution, source apportionment and ecological risk assessment of heavy metals in the sediments of Haizhou Bay national ocean park, China. *Marine Pollution Bulletin*, 149, 110651.

[55] Liu, J, Liu, S, Huang, Z, Fu, Y, Fei, J, Liu, X, He, Z, 2020. Associations between the serum levels of PFOS/PFOA and IgG N-glycosylation in adult or children. Environ. Pollut.

[56] Liu, W, He, W, Wu, J, Wu, W, Xu, Fu, 2019. Effects of fluorescent dissolved organic matters (FDOMs) on perfluoroalkyl acids (PFAAs) in lake and river water. Science of The Total Environment, 666, 598-607.

[57] Liu, W-X, He, W, Wu, J, Wu, W, Xu, F, 2019. Effects of fluorescent dissolved organic matters (FDOMs) on perfluoroalkyl acids (PFAAs) in lake and river water. Sci. Total Environ., 666, 598-607.

[58] Loccisano, A. E., Campbell, J. L. Jr., Andersen, M. E., Clewell, H. J. III. (2011). Evaluation and prediction of pharmacokinetics of PFOA and PFOS in the monkey and human using a PBPK model. *Regulatory Toxicology Pharmacology*, 59, 157-175.

[59] L*ó*pez-Peacock, E. (1995). Physical Chemistry: A Practical Approach. 115-117.

[60] Luebker, D, York, R, Hansen, K, Moore, J, Butenhoff, J, 2005. Neonatal mortality from in utero exposure to perfluorooctanesulfonate (PFOS) in Sprague-Dawley rats: Dose-response, and biochemical and pharmacokinetic parameters. Tox., 215, 149-169.

[61] Lung Health Institute: The Cost of Lung Disease. (2014, October 17). Retrieved September 18, 2020, from https://lunginstitute.com/blog/the-cost-of-lung-disease/

[62] Marella, T. K., Saxena, A., Tiwari, A. (2020). Diatom mediated heavy metal remediation: A review. Bioresource Technology, 305, 123068

[63] McNab, I. R. (2017). Rotational Spectroscopy, Theory. Encyclopedia of Spectroscopy and Spectrometry (Third Edition), 978-987. https://doi.org/10.1016/B978-0-12-803224-4.00273-9

[64] McQuarrie, D. A. (2008). Quantum Chemistry (Second Edition). 271-275.

[65] Microwave Rotational Spectroscopy. (2020, August 15). https://chem.libretexts.org/@go/page/1839

[66] Naturwissenschaften, D. (2008). Large-Scale Coupled-Cluster Calculations. 20-21.

[67] Nguyen, N, Khera, R, Ohno-Machado, L, Sandborn, W, Singh, S, 2018. Annual Burden and Cost of Hospitalization for High-Need, High-Cost Patients with Chronic Gastrointestinal and Liver Diseases. Clinical Gastroenterology and Hepatology, 16, 1284-1292.

[68] Orbital Polarization Terms in Basis Sets. (2020, March 18). Retrieved October 11, 2021, from https://chem.libretexts.org/@go/page/210882

[69] Oxford University Press. (2021). Overview ab-initio calculation. Retrieved from: https://www.oxfordreference.com/view/10.1093/oi/authority.20110803095344143

[70] Papajak, E., Zheng, J., Xu, X., Leverentz, H. R., Truhlar, D. G. (2011). Perspectives on Basis Sets Beautiful: Seasonal Plantings of Diffuse Basis Functions. Journal of Chemical Theory and Computation. https://doi.org/10.1021/ct200106a

[71] Particle in a 3-Dimensional box. (2019, April 11). Retrieved October 9, 2021, from https://chem.libretexts.org/@go/page/1726

[72] Peng, L., Chen, W., Li, M., Bai, Y., Pan, Y. (2014). GIS-based study of the spatial distribution suitability of livestock and poultry farming: The case of Putian, Fujian, China. Computers and Electronics in Agriculture, 108, 183-190.

[73] Peterson, K. Gaussian basis sets for molecular calculations (correlation consistent basis sets). http://tyr0.chem.wsu.edu/~kipeters/Pages/ccbasis.html

[74] PFAS Test and Response Kit. Retrieved September 18, 2020, from https://freshwaterfuture.org/community-resources/water-testing/

[75] Q-chem inc. (2020). Q-Chem 5.3 User's Manual. Ch. 8, 583.

[76] Rovibrational Spectroscopy. (2020, August 15). Retrieved September 25, 2021, from https://chem.libretexts.org/@go/page/1841

[77] Rovira, J, Martinea, Raju, Sharma, R, Nadal, T, Danae, V, Vassiliadou, C, Leondiadis, L, Domingo, J, Schuhmacher, M, 2019. Prenatal Exposure to PFOS and PFOA in Pregnant Women Cohor of Catalonia, Spain. Environ. Research, 175, 384-392.

[78] Schmitt, M., Meerts, L. (2018). Structures and Dipole Moments of Molecules in Their Electronically Excited States. Frontiers and Advances in Molecular Spectroscopy, 143-193.

[79] Sergi, C, 2019. Perfluorooctanoic Acid-A water and Oil Repellent. Encyclopedia of Environmental Health (Second Edition), 92-95.

[80] Sherrill, D. C. (2000). An Introduction to Hartree-Fock Molecular Orbital Theory. http://vergil.chemistry.gatech.edu/notes/hf-intro/hf-intro.pdf

[81] Silbey, R., Alberty, R., Bawendi, M. (2005). Physical Chemistry (4th Edition). 329-331.

[82] Silbey, R., Alberty, R., Bawendi, M. (2005). Physical Chemistry (4th Edition). 397-398.

[83] Srivastava, R. (2019) The Role of Proton Transfer on Mutations. Theoretical and Computational Chemistry. https://doi.org/10.3389/fchem.2019.00536

[84] Stedwell C.N., Polfer N.C. (2013) Spectroscopy and the Electromagnetic Spectrum. In: Polfer N., Dugourd P. (eds) Laser Photodissociation and Spectroscopy of Mass-separated Biomolecular Ions. Lecture Notes in Chemistry, vol 83. Springer, Cham.

[85] Stephens*, P.J., Devlin, F.J., Chabalowski, C.F., Frisch, M.J. (1994). *Ab Initio* Calculation of Vibrational Absorption and Circular Dichroism Spectra Using Density Functional Force Fields. Physical Chemistry, 98, 45, 11623-11627. https://doi.org/10.1021/j100096a001

[86] Strinati, G.C. (2005). Hartree and Hartree-Fock Methods in Electronic Structure. Encyclopedia of Condensed Matter Physics, 311-318.

[87] Struve, W. S. (1989). Fundamentals of Molecular Spectroscopy. 83-87.

[88] Sugden, T.M., Kennedy, C.N. (1965). Microwave Spectroscopy of Gasses.

[89] Sujitha, S. B., Jonathan, M. P., Villegas, L. E. C., Hernández-Camacho, C. J. (2020). Occurrences and ecotoxicological risks of trace metals in the San Benito Archipelago, Eastern Pacific Ocean, Mexico. *Ocean & Coastal Management*, 184, 105003.

[90] Sun, J, Chen, Y, Zhang, Z, Wang, P, Song, X, Wei, X, Feng, B, 2015. The spatio-temporal variations of surface water quality in China during the "Eleventh Five-Year Plan." *Environ. Monit. Assess.*, 187, 64.

[91] Szabo, A., Ostlund, N.,(1996). Modern Quantum Chemistry Introduction to Advanced Electronic Structure Theory. Dover Publications Inc.

[92] Testing Your Blood for PFAS. (2019, August 27) Retrieved September 18, 2020 from https://www.health.state.mn.us/communities/environment/hazardous/docs/pfas/indbltest.pdf

[93] Thakkar, A. (2014). Quantum Chemistry. 6-1-6-5.

[94] The Energy Levels of a Rigid Rotor. (2021, October 20). https://chem.libretexts.org/@go/page/13422

[95] The Selection Rule for the Rigid Rotor. (2021, May 11). Retrieved October 8, 2021, from https://chem.libretexts.org/@go/page/13675

[96] Toulouse, J. (2019). Introduction to perturbation theory and coupled-cluster theory for electron correlation. 5-10. http://www.lct.jussieu.fr/pagesperso/toulouse/enseignement/introduction_pt_cc.pdf

[97] Townes, C.H., Schawlow, A.L. (1955). Microwave Spectroscopy Dover Publication Inc. 2012.

[98] UN High Commissioner for Refugees (UNHCR), *The Sustainable Development Goals and Addressing Statelessness*, March 2017, available at: https://www.refworld.org/docid/58b6e3364.html [accessed 10 September 2020]

[99] Uwayezu, J., Yeung, L., Backstrom, M. (2022). Sorption of Perfluorooctane sulfonate (PFOS) including its isomers on hydrargillite as a function of pH, humic substances and Na_2SO_4. *Journal of Environmental Sciences*, 111, 263-272.

[100] Wang, B, Xie, L, Sun, X, 2011. Water Quality in Marginal Seas off China in the Last Two Decades. *International Journal of Oceanography*.

[101] Wang, Q, Zhao, Z, Ruan, Y, Li, J, Sun, H, Zhang, G, 2018. Occurrence and distribution of perfluorooctanoic acid (PFOA) and perfluorooctanesulfonic acid (PFOS) in natural forest soils: A nationwide study in China. Science of The Total Environment, 645, 596-602.

[102] Wang, S., Wang, H., Zhao, W., Cao, Y., Wan, Y. (2015). Investigation on the distribution and fate of perfluorooctane sulfonate (PFOS) and perfluorooctanoate (PFOA) in a sewage-impacted bay. *Environtal Pollution*, 205, 186-198.

[103] Wei, W., Ma, R., Sun, Z., Zhou, A., Bu, J., Long, X., & Liu, Y. (2018). Effects of Mining Activities on the Release of Heavy Metals (HMs) in a Typical Mountain Headwater Region, the Qinghai-Tibet Plateau in China. *International journal of environmental research and public health*, *15*(9), 1987.

[104] Whittaker, A. G., Mount, A. R., Heal M.R. (2000). Instant Notes Physical Chemistry. 315-321.

[105] Wilson, E. B. Jr. (1968). Microwave Spectroscopy in Chemistry. Science, 162(3849), 59-66. http://www.Jstor.org/stable/1725463.

[106] Y. Shao, Z. Gan, E. Epifanovsky, A. T. B. Giblert, M. Wormit, J. Kussmann, A. W. Lange, A. Behn, J. Deng, X. Feng, D. Ghosh, M. Goldey, P. R. Horn, L. D. Jacobson, M. A. B. Rohrdanz, R. P. Steele, E. J. O. Beran, Y. A. Bernard, E. Berguist, K. Brandhorst, K. B. Bravava, S. T. Brown, D. Casanova, C. -M. Chang, Y. Chen, S. H. Chien, K. D. Closser, D. L. Crittenden, M. Diendenhofen, R. A. DiStasio Jr, H. Dop, A. D. Dutoi, R. G. Edgar, S. Fatehi, L. Fusti-Molnar, A Ghysels, A. Golubeva-Zadorozhava, J. Gomes, M. W. D. Hanson-Heine, P. H. P. Harbach, A. W. Hauser, E. G. Hohenstein, Z. C. Holden, T. -C. Jagau, H. Ji, B. Kaduk, K. Khistvaev, J. Kim, J. Kim, R. A. King, P. Kluzinger, D. Kosenkow, T. Kowalczyk, C. M. Krauter, K. U. Lao, A. Laurent, K. V. Lawler, S. V. Levchenko, C. Y. Lin, F. Liu, E. Livshits, R. C. Lochan, A. Luenser, P. Manochar, S. F. Manzer, S. -P. Mao, N. Mardirossian, A. V. Marenich, S. A. Maurer, N. J. Mayhall, C. M. Oana, R. Olicares-Amaya, D. P. O'Neil, J. A. Parkhill, T. M. Perrine, R. Peverati, P. A. Pieniazek, A. Prociuk, D. R. Rehn, E. Rosta, N. J. Russ, N. Sergueev, S. M. Sharada, S. Sharmaa, D. W. Small, A. Sodt, T. Stein, D. Stück, Y. -C. Su, A. J. W. Thom, T. Tsuchimochi, L. Vogt, O. Vydrov, T. Wang, M. A. Watson, J. Wenzel, A. Qhite, C. F. Williams, V. Vanovschi, S. Yaganeh, S. R. Yost, Z. -Q. You, I. Y. Zhang, X. Zhang, Y. Zhou, B. R. Brooks, G. K. L. Chan, D. M. Chipman, C. J. Cramer, W. A. Goddard III, M. S. Gordon, W. J. Hebre, A. Klamt, H. F. Schaefer III, M. W. Schmidt, C. D. Sherrill, D. G. Truhlar, A. Warshel, X. Xua, A. Aspuru-Guzik, R. Baer, A. T. Bell, N. A. Besley, J. -D. Chai, A. Dreuw, B. D. Dunietz, T. R. Furlani, S. R. Gwaltney, C. -P. Hsu, Y. Jung, J. Kong, D. S. Lambrecht, W. Liang, C. Ochsenfeld, V. A. Rassoloy, L. V. Slipchenko, J. E. Subotnik, T. Van Voorhis, J. M. Herbert, A. I. Kryloy, P. M. W. Gill, and M. Head-Gordon. Advances in molecular quantum chemistry contained in the Q-Chem 4 program package.

[107] Yamashita, N., Kannan, K., Taniyasu, S., Horii, Y., Petrick, G., Gamo, T., 2005. A global survey of perfluorinated acids in oceans. Mar. Pollut. Bull., 51, 658-668

[108] Yang, L., He, L., Xue, J., Ma, Y., Xie, Z., Wu, L., Huang, Z., 2020. Persulfate-based degradation of perfluorooctanoic acid (PFOA) and perfluorooctane sulfonate (PFOS) in aqueous solution: Review on influences, mechanisms and prospective. J. Hazard. Mater., 393, 122405.

[109] Young, D. 2001.The Absolute Beginners Guide to Gaussian. http://www.ccl.net/cca/documents/dyoung/topics-orig/contents.html

[110] Yue, Y, Li, S, Q, Pereira, R, Lee, J, Doherty, J, Zhang, Z, Peng, Y, Clark, J, Timme-Laragy, A, Park, Y, 2020. Perfluorooctanesulfonic acid (PFOS) and perfluorobutanesulfonic acid (PFBS) impaired reproduction and altered offspring

physiological functions in Caenorhabditis elegans. Food and Chemical Toxicology, 145, 111695.

[111] Yukioka, S, Tanaka, S, Suzuki, Y, Echigo, S, Karrman, A, Fujii, S, 2020. A profile analysis with suspect screening of per- and polyfluoroalkyl substances (PFASs) in firefighting foam impacted waters in Okinawa, Japan. Water Research, 184, 116207.

[112] Zareitalabad, P, Siemens, J, Hamer, M, Amelung, W, 2013. Perfluorooctanoic acid (PFOA) and perfluorooctanesulfonic acid (PFOS) in surface waters, sediments, soils and wastewater – A review on concentrations and distribution coefficients. Chemos., 91, 725-732.

[113] Zeng, Z, Song, B, Xiao, R, Zeng, G, Gong, J, Chen, M, Xu, P, Zhang, P, Shen, M, Yi, H, 2019. Assessing the human health risks of perfluorooctane sulfonate by in vivo and in vitro studies. Environment International, 126, 598-610.

[114] Zheng, S., Wang, Q., Yuan, Y., Sun, W. (2020). Human health risk assessment of heavy metals in soil and food crops in the Pearl River Delta urban agglomeration of China. *Food Chemistry*, 316, 126213.

[115] Zeng, Z, Song, B, Xiao, R, Zeng, G, Gong, J, Chen, M, Xu, P, Zhang, M, Yi, H, 2019. Assessing the human health risks of perfluorooctane sulfonate by in vivo and in vitro studies. Environment Internantional, 126, 598-610.

[116] Zhang, Y. I., Grüneis, A. (2019). Coupled Cluster Theory in Materials Science. Frontiers in Materials, 6, 123. https://www.fronteirsin.org/article/10.3389/fmats.2019.00123

APPENDIX

APPENDIX

REFERENCES FOR FIGURES IN CHAPTER 1

Figure 2:

[1] Liu, J., Liu, S., Huang, Z., Fu, Y., Fei, J., Liu, X., & He, Z. (2020). Associations between the serum levels of PFOS/PFOA and IgG N-glycosylation in adult or children. *Environmental pollution (Barking, Essex : 1987)*, *265*(Pt A), 114285.

[2] Li, R., Guo, C., Lin, X., Chan, T. F., Lai, K. P., & Chen, J. (2020). Integrative omics analyses uncover the mechanism underlying the immunotoxicity of perfluorooctanesulfonate in human lymphocytes. *Chemosphere*, *256*, 127062.

[3] Zeng, Z., Song, B., Xiao, R., Zeng, G., Gong, J., Chen, M., Xu, P., Zhang, P., Shen, M., & Yi, H. (2019). Assessing the human health risks of perfluorooctane sulfonate by in vivo and in vitro studies. *Environment international*, *126*, 598–610.

[4] Loccisano, A. E., Campbell, J. L., Jr, Butenhoff, J. L., Andersen, M. E., & Clewell, H. J., 3rd (2012). Evaluation of placental and lactational pharmacokinetics of PFOA and PFOS in the pregnant, lactating, fetal and neonatal rat using a physiologically based pharmacokinetic model. *Reproductive toxicology (Elmsford, N.Y.)*, *33*(4), 468–490.

[5] Kuehl, D. Haebler, R. Potter, C. Lahvis, G. Michael, D. Regal, R. (2009). PFOS and PFOSA in bottlenose dolphins: An investigation into two unusually high mortality epizootics. Reproductive Toxicology, 27, 421.

Figure 3:

[1] EFSA, European Food Safety Authority (2012). Perfluoroalkylated substances in food: occurrence and dietary exposure EFSA J, 10, pp. 2743 – 2798 (41)

Figure 4:

[1] Arrieta-Cortes, R, Fabrias, P, Hoyo-Vadillo, C, Kleiche-Dray, M, 2017. Carcinogenic risk of emerging persistent organic pollutant perfluorooctane sulfonate (PFOS): A proposal of classification. Reg. Tox. and Pharm., 83, 66-80.

Figure 5:

[1] M. Ruzek, 1999

Figure 6:

[1] PFAS Test and Response Kit. Retrieved September 18, 2020, from https://freshwaterfuture.org/community-resources/water-testing/

[2] Laboratory Testing. Retrieved September 18, 2020, from https://www.michigan.gov/pfasresponse/0,9038,7-365-86704_90691---,00.html

[3] Testing Your Blood for PFAS. (2019, August 27) Retrieved September 18, 2020 from https://www.health.state.mn.us/communities/environment/hazardous/docs/pfas/indbltest.pdf

Figure 7:
[1] Nguyen, N, Khera, R, Ohno-Machado, L, Sandborn, W, Singh, S, 2018. Annual Burden and Cost of Hospitalization for High-Need, High-Cost Patients with Chronic Gastrointestinal and Liver Diseases. Clinical Gastroenterology and Hepatology, 16, 1284-1292.
[2] Heart Disease Facts. (2020, September 08). Retrieved September 18, 2020, from https://www.cdc.gov/heartdisease/facts.htm
[3] Lung Health Institute: The Cost of Lung Disease. (2014, October 17). Retrieved September 18, 2020, from https://lunginstitute.com/blog/the-cost-of-lung-disease/

Figure 8:
[1] Lerner, S. (2018, July 31). 3M Knew About the Dangers of PFOA and PFOS Decades Ago, Internal Documents Show. Retrieved September 18, 2020, from https://theintercept.com/2018/07/31/3m-pfas-minnesota-pfoa-pfos/
[2] Business & Human Rights Resource Centre. (n.d.). Retrieved September 18, 2020, from https://www.business-humanrights.org/en/latest-news/dupont-lawsuits-re-pfoa-pollution-in-usa/

Figure 10
[1] UN High Commissioner for Refugees (UNHCR), *The Sustainable Development Goals and Addressing Statelessness*, March 2017, available at: https://www.refworld.org/docid/58b6e3364.html [accessed 10 September 2020]

CHAPTER 2 SUPPLEMENTAL MATERIAL

Table 10. Seawater Quality Standards of China in mg/L (GB 3097, 1997) [5]

Item	**Clean water (Category I)**	**Relatively clean water (Category II)**	**Slightly polluted water (Category III)**		**Medium polluted water (Category IV)**	**Heavily polluted water (inferior to Category IV)**
Dissolved Oxygen	**> 6**	**> 5**	**> 4**		**> 3**	**< 3**
Chemical Oxygen Demand (COD)	**≤ 2**	**≤ 3**	**≤ 4**		**≤ 5**	**≥ 5**
Biochemical Oxygen Demand (BOD5)	**≤ 1**	**≤ 3**	**≤ 4**		**≤ 5**	**≥ 5**
Inorganic Nitrogen (as N)	**≤ 0.20**	**≤ 0.30**	**≤ 0.40**		**≤ 0.50**	**≥ 0.50**
Phosphate (as P)	**≤ 0.015**	**≤ 0.030**		**≤ 0.045**		**≥ 0.045**

Mercury	**≤ 0.00005**	**≤ 0.0002**		**≤ 0.0005**		**≥ 0.0005**
Cadmium	**≤ 0.001**	**≤ 0.005**		**≤ 0.010**		**≥ 0.010**
Lead	**≤ 0.001**	**≤ 0.005**	**≤ 0.010**		**≤ 0.050**	**≥ 0.050**
Chromium (VI)	**≤ 0.005**	**≤ 0.010**	**≤ 0.020**		**≤ 0.050**	**≥ 0.050**
Total Chromium	**≤ 0.05**	**≤ 0.10**	**≤ 0.20**		**≤ 0.5**	**≥ 0.50**
Arsenic	**≤ 0.020**	**≤ 0.030**		**≤ 0.050**		**≥ 0.050**
Copper	**≤ 0.005**	**≤ 0.010**		**≤ 0.050**		**≥ 0.050**
Zinc	**≤ 0.020**	**≤ 0.050**	**≤ 0.10**		**≤ 0.50**	**≥ 0.50**
Oil	**≤ 0.05**	**≤ 0.30**		**≤ 0.50**		**≥ 0.50**

Table 11. Surface Water Quality Standards of China for Heavy Metals in μg/L (GB 3838, 2002)

Water Standard	**As**	**Mn**	**Cr**	**Ni**	**Cu**	**Cd**	**Pb**	**Zn**
Grade I [a]	**10**	**-**	**10**	**-**	**10**	**1**	**10**	**50**
Drinking [b]	**10**	**100**	**10**	**20**	**1000**	**5**	**10**	**1000**

Table 12. Surface Water Quality Standards of China for Ammonia Nitrogen in mg/L (GB 3838, 2002).

Water Quality		**Excellent**	**Good**	**Slightly Polluted**	**Polluted**	**Severely Polluted**
General Water Quality Class		**I**	**II**	**III**	**IV**	**V**
Dissolved Oxygen	**≥**	**Saturation rate 90% or 7.5**	**6**	**5**	**3**	**2**
Permanganate Index	**≤**	**2**	**4**	**6**	**10**	**15**
Ammonia Nitrogen	**≤**	**0.15**	**0.5**	**1.0**	**1.5**	**2.0**

Table 13 Surface Water Quality Standards of China for Oil and Mercury in mg/L (GB 3838, 2002)

Level	**I**	**II**	**III**	**IV**	**V**	**Normal Change**
DO	**7.5**	**6**	**5**	**3**	**2**	**-1.0~1.0**
COD_{Mn}	**2**	**4**	**6**	**10**	**15**	**-2.0~2.0**
BOD_5	**3**	**5**	**4**	**6**	**10**	**-1.0~1.0**
NH_3-N	**0.15**	**0.05**	**1.00**	**1.5**	**2.00**	**-0.35~0.35**
Pb	**0.01**	**0.01**	**0.05**	**0.05**	**1**	**-0.04~0.04**
Hg	**0.00005**	**0.00005**	**0.001**	**0.001**	**0.001**	**$-5x10^{-5}$~$5x10^{-5}$**
Oil	**0.05**	**0.05**	**0.05**	**0.5**	**1.0**	**-0.45~0.45**
Volatile phenols	**0.002**	**0.002**	**0.005**	**0.01**	**0.1**	**-0.003~0.003**

Table 14. Surface Water Quality Standards of China for Total Nitrogen and Total Phosphorus in mg/L (GB 3838, 2002)

Index	Class III	Class IV	Class V
DO	5	3	2
NH3-N	1	1.5	2
TN	1	1.5	2
TP	0.05	0.1	0.2
BOD5	4	6	10
COD	20	30	40

Table 15. Surface Water Quality Standards of China for Fluoride (Category III) in mg/L (GB 3838, 2002)

Sampling point	pH value	Phosphate (mg/L)	Fluoride (mg/L)	Cyanide (mg/L)	Volatile Phenols (mg/L)	Arsenic (mg/L)	Element Phosphorus (mg/L)
Water quality standard for fisheries (GB 11607-1989)	6.5 - 8.5		≤ 1	≤ 0.005	≤ 0.005	≤ 0.05	≤ 0.001
Environmental quality standards for surface water (GB 3838-2002) III	6 - 9	0.2 (TP)	≤ 1.0	≤ 0.2	≤ 0.005	≤ 0.05	
Industrial water of Siying Coal Mine 1	7.68	0.164	-	1.62	-	-	0.0265
Industrial water of Siying Coal Mine 2	7.81	0.258	-	3.85	-	-	0.0299
Phosphorus sludge waste liquid 1	3.3	2270	274	45.00	0.750	0.034	20.03
Phosphorus sludge waste liquid 2	3.3	2343	230	44.64	1.25	0.032	12.99
Remnant water in the washed pit	9.45	0.021	0.12	-	-	-	0.0009

BIOGRAPHICAL SKETCH

Karla Veronica Salazar's personal email is karlasalazar64@hotmail.com. She started on her education in Matamoros, Mexico when undergoing pre-school and first grade. As she was entering second grade, she moved to Brownsville, Texas to study at Yturria Elementary to complete her elementary school education. Following elementary, she went to Stillman Middle School where she entered band class as an elective to learn to play the flute. It was in middle School where she met her middle school sweetheart and now-fiance who is also celebrating a Completion of education in a master's degree in chemistry as well. Following middle school, it Came high school where she underwent Veterans Memorial Early College High School. During This time, she was still in band and trying to get as many college courses as possible in the bag To start on her early college education. Karla graduated high school in the summer of 2017, and Started college at the University of Texas Rio Grande Valley pursuing a bachelor's degree in Chemistry. During sophomore year of college, Karla started working in a pharmacy to earn money to help pay school expenses. Following lots of hard work, Karla obtained her bachelor's degree of science in the field of chemistry in December 2019. Without a college break, she went straight into her Master's Degree and two years later completed her Master's Degree of Science in Chemistry.